

SHIP RESISTANCE AND PROPULSION

TABLE OF CONTENTS

	Page
1. Similarity Theory and Phenomenological Methods.	2
1.1 Forms of resistance.	2
1.2 Dynamic similarity.	3
1.3 Resistance calculations.	5
2. Ship Resistance.	7
2.1 Frictional resistance.	7
2.2 Wave making resistance.	10
2.3 Other components of resistance.	13
2.4 Relation of hull form to resistance.	18
3. Ship Propulsion.	21
3.1 Powering of ships.	21
3.2 Propeller action.	22
3.3 Law of similitude for propellers.	23
3.4 Hull propeller interaction.	26
3.5 Cavitation.	28
3.6 Propeller selection and design.	31
List of Figures.	36
List of Tables.	37

1. Similarity Theory and Phenomenological Methods.

A ship differs from land based large engineering structures in that, in addition to all its other functions, it must be designed to move efficiently through the water with a minimum of external assistance. In Part I it has been shown how the engineer can ensure adequate buoyancy and stability for a ship, intact or damaged. In Part II the problem of providing adequate structure for the support of the ship and its contents, both in calm water and rough seas was discussed.

In this part we are concerned with the problems of ship resistance and propulsion. The task at hand is to ensure that, within the limits of other design requirements, the hull form and propulsion arrangement will be the most efficient in the hydrodynamic sense. The ultimate test is that the ship shall perform at the required speed with the minimum of shaft power, and the problem is to attain the best combination of low resistance and high propulsive efficiency. In general this can only be attained by a proper matching of hull, engine, and propeller.

Another factor that influences the hydrodynamic design of a ship is the need to ensure not only good calm water performance but also that under average service conditions at sea the ship shall not suffer from excessive motions, wetness of decks, or excessive speed loss. The assumption that a hull form that is optimum in calm waters will also be optimum in rough seas is not necessarily valid. Furthermore, a ship must be able to control its direction at will and keep its desired path through the water. The problem of ship motions, attainable speed and added power requirements in waves, as well as maneuverability and controllability are discussed in Part IV.

In Section 1 we approach ship resistance through an intuitive or phenomenological sense, while more rational fluid mechanics considerations are reserved for Section 2. Ship propulsion, propulsive efficiency, and propeller selection are discussed in Section 3.

1.1 Forms of resistance.

The resistance of a ship at a given speed is the force required to tow the ship at that speed in smooth water, assuming no interference from the towing ship. If the hull has no appendages, this is called the *bare-hull* or *towing* resistance, and although very near to, it is not exactly the same as the *propulsion* resistance due to hull/propeller interactions.

This total resistance is made up of a number of different components, which are caused by a variety of factors and which interact with each other in a rather complex fashion. In order to deal with the question more efficiently, it is customary to consider the total *calm* water resistance as being made up of four main components.

(a) *Frictional* resistance, due to the motion of the hull through a viscous fluid.

(b) *Wave making* resistance, due to the energy that must be supplied continuously by the ship to the wave system created on the free surface.

(c) *Eddy* resistance, due to the energy carried away by eddies shed from the hull or appendages. This is especially severe at the stern where the water may be unable to follow the curvature and will break away from the hull, giving rise to eddies and separation resistance.

(d) *Air* resistance experienced by the above-water part of the main hull and the super-

structures due to the motion of the ship through the air.

The resistances under (b) and (c) are commonly considered together (although they arise from different physical mechanisms) under the name *residuary* resistance. Also a variety of other forms of resistance exists such as added resistance due to waves and the wave breaking resistance for a ship sailing in a seaway, and the added resistance due to turning (for surface ships) and diving (for submarines). These are mentioned in the next part of the notes, under ship dynamics.

A streamlined body moving in a straight horizontal line at constant forward speed, deeply immersed in an unlimited ocean, presents the “simplest” (still far from trivial) case of resistance. Since there is no free surface, there is no wave formation and therefore no wave making resistance. For an ideal fluid the velocity distribution past the hull will be greater than the speed of advance along the midportion, and in the region of bow and stern will be less, as shown in Figure 1. The pressure distribution as derived from Bernoulli’s law will follow the inverse pattern: higher at the bow and stern, and lower in the middle. Since the fluid is assumed to be without viscosity, the pressure forces will everywhere be normal to the hull, and it can be shown that they will cancel out each other and the body will experience no resistance (d’Alembert’s paradox).

In a real fluid, the boundary layer alters the virtual shape and length of the body, the pressure distribution at the stern is changed and its forward component is reduced. In this case there is a net force on the body acting against the motion, giving rise to a resistance which is variously referred to as *form drag* or viscous pressure drag. The body also experiences frictional resistance and perhaps eddy resistance as well. The fluid immediately in contact with the surface of the body is carried along with the surface, and that in the close vicinity is set in motion in the same direction as that in which the body is moving. This results in a boundary layer which gets gradually thicker from the bow to the stern, and in which the velocity varies from that of the body at its surface to that appropriate to the potential flow pattern at the outer edge of the layer. The momentum supplied to the water in the boundary layer by the hull is a measure of the frictional resistance. If the body is rather blunt at the after end the flow may detach at some point, called the *separation point*, thus reducing the total pressure on the afterbody and adding to the resistance. This separation resistance is evidenced by a pattern of eddies which is a drain of energy.

A ship moving on the surface of the sea experiences all of the above forms of resistance in much the same way as does a submerged body. However, the presence of the free surface adds a further component. The resulting pressure distribution on the hull results in the creation of a wave system which spreads out astern of the ship and has to be continuously recreated. This corresponds to a drain of energy supplied by the ship and is termed the wave making resistance.

A plot of the total resistance (effective horsepower, EHP, per ton of displacement) versus the speed-length ration V/\sqrt{L} (V in knots, L in feet) for different types of ships is presented in Figure 2.

1.2 Dynamic similarity.

Dimensional analysis which is the basis for similarity theory, is essentially a means of utilizing a partial knowledge of a problem when the details are too obscure to permit an

exact analysis. Dimensional analysis methods do not yield numerical answers, but they provide the form of the answer so that an experiment can be used to the fullest advantage in determining a general empirical solution. The method rests on the basic principle that every equation which expresses a physical relationship must be dimensionally homogeneous. There are three basic quantities in mechanics — mass, length, and time — which are represented by the symbols M , L , and T . All other quantities have dimensions made up from these three basic ones.

Now consider the case of a ship moving with constant velocity V on the free surface. Geometrical similarity is assumed with the geometry of the hull characterized by its length L . Since the steady motion of the ship on the free surface generates a system of waves dependent on the gravitational acceleration g , this parameter must be included in the dimensional analysis along with the length L , velocity V , density ρ , and kinematic viscosity of the water ν . If we assume now that the resistance R takes the form of a power law in terms of the above variables, we have

$$R \propto \rho^a V^b L^c \nu^d g^e . \quad (1)$$

For equation (1) to be dimensionally consistent we must have

$$\frac{ML}{T^2} = \left(\frac{M}{L^3}\right)^a \left(\frac{L}{T}\right)^b L^c \left(\frac{L^2}{T}\right)^d \left(\frac{L}{T^2}\right)^e , \quad (2)$$

and from equation (2) we get

$$\begin{aligned} a &= 1 , \\ -3a + b + c + 2d + e &= 1 , \\ -b - d - 2e &= -2 , \end{aligned}$$

or

$$\begin{aligned} a &= 1 , \\ b &= 2 - d - 2e , \\ c &= 2 - d + e . \end{aligned}$$

Then equation (1) becomes

$$R \propto \rho V^2 L^2 \left(\frac{VL}{\nu}\right)^{-d} \left(\frac{gL}{V^2}\right)^e . \quad (3)$$

Remembering now that we started with geometrically similar bodies, L^2 is proportional to the wetted surface S , and equation (3) may be written

$$\frac{R}{1/2\rho SV^2} = f\left(\frac{VL}{\nu}, \frac{gL}{V^2}\right) , \quad (4)$$

where the left hand side is the nondimensional resistance coefficient C_R .

Therefore, the ship resistance is

$$R = \frac{1}{2}\rho C_R V^2 S , \quad (5)$$

where the resistance coefficient

$$C_R = C_R(\text{Re}, \text{Fn}) ,$$

is a function of the *Reynolds* number

$$\text{Re} = \frac{VL}{\nu} , \quad (6)$$

and the *Froude* number

$$\text{Fn} = \frac{V}{\sqrt{gL}} . \quad (7)$$

It can be seen that the method of dimensional analysis has revealed here the two important parameters in ship resistance: (i) the Reynolds number (6) which physically represents the ratio of inertial forces to viscous forces in the fluid; and (ii) the Froude number (7) which is the ratio of inertia forces to gravity forces. Two geometrically similar hull forms (geosims) with the same Re *and* Fn will have the same resistance coefficient C_R . Unfortunately, this is an impossible task, as we will see in the next section.

1.3 Resistance calculations.

In principle one can get the resistance coefficient C_R by solving the complete set of Navier–Stokes equations for a three dimensional body moving on the free surface: a formidable task. Even in these CRAY–zy days of numerical ship hydrodynamics this is not reliably possible; experiments in model tanks are still necessary. If the subscript s corresponds to the ship and m to the geosim model, in order to have

$$(C_R)_s = (C_R)_m , \quad (8)$$

we must ensure that

$$(\text{Re})_s = (\text{Re})_m \quad \text{or} \quad \frac{V_m}{V_s} = \frac{L_s}{L_m} \cdot \frac{\nu_m}{\nu_s} , \quad (9)$$

and

$$(\text{Fn})_s = (\text{Fn})_m \quad \text{or} \quad \frac{V_m}{V_s} = \left(\frac{g_m}{g_s} \right)^{1/2} \left(\frac{L_m}{L_s} \right)^{1/2} . \quad (10)$$

Now a reasonable model to ship length ratio would be $(L_m/L_s) = (1/100)$, and equations (9) and (10) require

$$\frac{V_m}{V_s} = 100 \frac{\nu_m}{\nu_s} \quad \text{and} \quad \frac{V_m}{V_s} = \frac{1}{10} \left(\frac{g_m}{g_s} \right)^{1/2} .$$

We see that in order to satisfy both requirements (9) and (10) we must either (i) perform experiments in a space station with adjustable orbit and adjustable g ; or (ii) invent an exotic fluid with $\nu_m/\nu_s = 1/1000$. Since neither is possible, we cannot satisfy both Re and Fn scaling at the same time. If we call $L_s/L_m = \lambda$, we can either satisfy

$$(\text{Re})_s = (\text{Re})_m \quad \Rightarrow \quad \frac{V_m}{V_s} = \lambda , \quad \text{or} \quad (11)$$

$$(\text{Fn})_s = (\text{Fn})_m \quad \Rightarrow \quad \frac{V_m}{V_s} = \frac{1}{\sqrt{\lambda}} , \quad (12)$$

for the same fluid for the ship and the model. Now since $\lambda \gg 1$, Re scaling according to (11) is highly impractical, and the best we can do is Froude number scaling according to (12).

So the problem now is how to get $(C_R)_s$ from measurements of $(C_R)_m$ by assuming experiments at Froude number scaling only. Strictly speaking, since C_R is a function of both Re and Fn, this is not possible. Froude's hypothesis comes here to the rescue (as early as 1868). Write C_R as in

$$C_R(\text{Re}, \text{Fn}) = C_F(\text{Re}) + C_r(\text{Re}, \text{Fn}) , \quad (13)$$

where C_F is the frictional resistance coefficient which is a function of Re number only according to the physical motivations of Section 1.1, and the rest is the residual resistance coefficient. The latter is written as

$$C_r(\text{Re}, \text{Fn}) = C_W(\text{Fn}) + C_{\text{FORM}}(\text{Re}, \text{Fn}) , \quad (14)$$

where C_W is the wave making resistance coefficient (the main part of C_r) which depends on Fn only, and C_{FORM} is the form drag coefficient. The form drag has very little to do with Fn, and it is fortunate that it has little to do with Re too. It is a constant and remains the same for geosims. Therefore, Froude's hypothesis follows in the form

$$C_R(\text{Re}, \text{Fn}) = C_F(\text{Re}) + C_W(\text{Fn}) + C_{\text{FORM}} . \quad (15)$$

Before proceeding any further, an experimental validation of Froude's hypothesis can be made by plotting C_R versus Re, for different values of the hull length. According to (15), all experimental points for the same Froude number should be situated at equal distances above the flat plate frictional resistance curve, and Froude's hypothesis can be evaluated according to the degree to which this is true. Numerous results on this have been obtained and confirm that Froude's method does succeed to a considerable extent in correlating the resistance of geosim ship hulls of widely different lengths. Therefore, so far we have achieved the following

- Construction of a geometrically similar model enforces $(C_{\text{FORM}})_s = (C_{\text{FORM}})_m$.
- Froude number scaling enforces $(C_W)_s = (C_W)_m$.
- We only need to compute C_F . But since ships look (still) rather slender, the frictional resistance should be approximately the same with that of a flat plate with the same wetted area.

The above procedure can be summarized as follows:

1. Test the model with Fn number scaling, $V_m = V_s/\sqrt{\lambda}$, where $\lambda = L_s/L_m$.
2. Measure the total resistance $(R_T)_m$.
3. Estimate the frictional resistance of the model $(R_F)_m$ by using flat plate results at the model's Reynolds number.
4. Compute the model residuary resistance from $(R_r)_m = (R_T)_m - (R_F)_m$.

5. Since $(C_r)_s = (C_r)_m$ we can find the ship residuary resistance by $(R_r)_s = \frac{1}{2}(C_r)_s \rho V_s^2 S_s$ or $(R_r)_s = \frac{1}{2}(C_r)_m \rho (V_m \sqrt{\lambda})^2 S_m \lambda^2 = \frac{1}{2}(C_r)_m \rho V_m^2 S_m \lambda^3$.
6. Estimate the frictional resistance of the ship $(R_F)_s$ by using flat plate results at the ship's Reynolds number.
7. Compute the total ship resistance by

$$(R_T)_s = (R_r)_s + (R_F)_s . \quad (16)$$

If we need the total ship resistance coefficient

$$(C_R)_s = (C_F)_s + (C_r)_s = (C_F)_s + (C_r)_m = (C_F)_s + (C_R)_m - (C_F)_m . \quad (17)$$

This method gives, except for very small models, satisfactory predictions for the resistance. Usually, towing tanks incorporate a correction factor, called correlation allowance C_A , so that equation (17) becomes

$$(C_R)_s = (C_F)_s + (C_R)_m - (C_F)_m + C_A , \quad (18)$$

where C_A is of the order of 0.0004. This correlation allowance, once called roughness coefficient, is used mainly to fine-tune model tests with full scale measurements. Physically it is due to a variety of factors, most notably the difference in roughness characteristics (the model surface is always smoother than the ship) and the laminar flow near the bow of the model (turbulence stimulators are often used on the model to alleviate this phenomenon).

2. Ship Resistance.

The simple qualitative arguments that were developed in the previous section are adequate for preliminary estimates of the total resistance of a ship from model tests. In this section we go a bit deeper into the problem in order to get some more understanding of the physical mechanisms which contribute to the resistance of a ship.

2.1 Frictional resistance.

The frictional resistance is usually the most significant component of the total ship resistance. For relatively slow ships with high block coefficients it contributes to about 85% of the total resistance, whereas for high speed streamlined displacement hulls it may drop to about 50%. These values may become higher in time due to the increased roughness of the ship surface. Froude's hypothesis was remarkable in the sense that he was able to split the total resistance coefficient in two parts that are weakly dependent upon each other. The dependence of frictional resistance on the Re number was not known during Froude's time and he was having some difficulty extrapolating his model tests to full scale. Nevertheless, his regression results were very meticulous and they were in use for quite a few decades.

And then came Osborne Reynolds, and more light was shed into the problem. We now know of the existence of a boundary layer for the fluid flow past a flat plate. The flow is

characterized as laminar for low Re numbers or turbulent for higher Re numbers (more usual in typical ship resistance problems). Turbulence is characterized by the superposition of a highly irregular and oscillatory velocity pattern upon an otherwise smooth flow. This results in a convection of momentum which causes the velocity profile to become more uniform, as shown in Figure 3, and it results ultimately in a larger velocity gradient and shear stress on the body surface. This causes an increase in the frictional resistance coefficient, as shown in Figure 4.

Theoretical considerations due to Prandtl and von Karman (the same von Karman from plate theory) led to the development of a theoretical formula for the frictional resistance coefficient of the form

$$\frac{A}{\sqrt{C_F}} = \log_{10}(\text{Re} \cdot C_F) + B . \quad (19)$$

Extensive sets of experimental data were analyzed by Schoenherr in the light of equation (19), and he found that he could get a good fit to the experimental data by making B zero and A equal to 0.242, so arriving at the well known Schoenherr formulation

$$\frac{0.242}{\sqrt{C_F}} = \log_{10}(\text{Re} \cdot C_F) , \quad (20)$$

which was adopted in 1947 by the ATTC (American Towing Tank Conference) for use with standard ship resistance computations. This ATTC line is shown in Figure 5 together with the incorporation of the allowance coefficient C_A . This coefficient, typically about 0.0004 as was mentioned in Section 1.3, varies for different ship types and model sizes. Current (1982) NAVSEA recommendation, based on sea trials, is

$$\begin{aligned} C_A &= 0.0008 & L < 190' \\ C_A &= \frac{0.0083}{L^{1/3}} - 0.00064 & 190' \leq L \leq 960' \\ C_A &= 0.0002 & 960' < L \end{aligned}$$

With the introduction of larger ships, and comparatively smaller models, it was observed that the correlation allowance C_A necessary to reconcile the ship resistance with the prediction from the model using the ATTC line was sometimes zero or negative, which was rather embarrassing. This was attributed to the fact that the Schoenherr line had a slope which was not considered to be sufficiently steep at the low Reynolds numbers appropriate to small models, so that it did not give good correlation between the results of small and large models. To alleviate this problem, the International Towing Tank Conference (ITTC) adopted in 1957 a new formula

$$C_F = \frac{0.075}{(\log_{10} \text{Re} - 2)^2} , \quad (21)$$

which is known as the ITTC line and is the current standard (see Figure 5). It is important to appreciate that this is a model/ship correlation line and *not* a frictional resistance line, it makes no pretense to represent the frictional resistance of plane or curved surfaces and should not be used for such a purpose.

Hughes in 1963 proposed a variation of (21) as

$$C_{FO} = \frac{0.066}{(\log_{10} \text{Re} - 2.03)^2} , \quad (22)$$

which is also shown in Figure 5. In association with line (22) which represents the frictional resistance coefficient C_{FO} in two dimensional flow, Hughes proposed a new method of extrapolation from model to ship. He assumed that the total model resistance coefficient C_{TM} could be divided into two parts, C_{VM} and C_{WM} , representing the viscous and wave making resistance, respectively, Figure 6. At low Froude numbers, C_{WM} will be vanishingly small, and at a point such as K_M the curve of C_{TM} will become approximately parallel to the friction line. Hughes called K_M the “run-in” point and $G_M K_M$ the viscous resistance coefficient C_{VM} . $G_M H_M$ is the two dimensional, flat plate resistance coefficient C_{FOM} given by equation (22), and $H_M K_M$ is the form resistance coefficient, due at least in part to the curvature of the hull. Now a form factor r can be defined by the expression

$$r = 1 + k = \frac{G_M K_M}{G_M H_M} = \frac{C_{VM}}{C_{FOM}},$$

so that

$$k = \frac{C_{VM} - C_{FOM}}{C_{FOM}}.$$

This form factor r is independent of the Reynolds number and is the same for all similar models and ships. In Figure 6 a series of lines is drawn whose ordinates are, respectively, 1.10, 1.20, . . . , times those of the C_{FO} curve, representing these constant values of the form factor r . In the example shown, the model resistance coefficient curve becomes parallel to the form factor curves at K_M , indicating that the model has a form factor of 1.25. The line $1.25C_{FO}$ then becomes the extrapolator for the particular hull form, and the ship curve of C_{TS} will start at a point K_S on this line, where K_M and K_S apply to the same value of Froude number for model and ship. The rest of the ship curve is obtained by plotting values of $C_{WS} = C_{WM}$ above the $1.25C_{FO}$ curve at the appropriate values of Fn.

Since in the Froude method the whole of the model residuary resistance coefficient C_R is transferred to the ship unchanged, whereas in the Hughes method that part of C_R attributed to viscous effects is reduced in the transfer, the Hughes method gives substantially lower ship predictions and so calls for larger values of the correlation allowance. This is a step towards avoiding the negative allowances sometimes found when using the Froude method. A further point of difference between the Froude and Hughes procedure is that whereas in the former case only the slope of the correlation line matters, in the latter the absolute vertical position of the line also affects the ship prediction, so that the determination of the basic line becomes an essential factor in the use of the Hughes method.

The essence of the Hughes method is that the C_{FORM} coefficient in equation (15) is written as

$$C_{FORM}(\text{Re}, \text{Fn}) = \eta C_F(\text{Re}), \quad (23)$$

instead of constant. As was indicated by Landweber a more general view of the issue suggests the form

$$C_{FORM} = \zeta + \eta C_F(\text{Re}), \quad (24)$$

where ζ and η are two parameters that can be adjusted to give Froude’s method ($\eta = 0$) or Hughes’ method ($\zeta = 0$).

Granville’s technique is sometimes used and it usually results in predictions that fall between Froude (high) and Hughes (low). Granville’s friction line was derived in 1977 and

is

$$C_{FO} = \frac{0.0776}{(\log_{10} \text{Re} - 1.88)^2} + \frac{60}{\text{Re}},$$

as shown in Figure 5.

It is obvious from the foregoing that the subject of ship/model correlation is still far from being closed. In general, one can say that the total resistance coefficient is

$$C_T = C_V + C_W, \quad (25)$$

where the wave making resistance coefficient is

$$C_W = C_W(\text{Fn}), \quad (26)$$

and the viscous resistance coefficient is

$$C_V = (1 + k)C_{V_0}(\text{Re})f(\text{Fn}). \quad (27)$$

Here, $C_{V_0}(\text{Re})$ is some basic frictional resistance curve and the form factor k can be established by velocity distribution measurements in the wake of the model. The coefficient $f(\text{Fn})$ can be established by measurements of the waves generated by the model (wave surveys or wave cuts). The (hopefully weak) dependence of C_V on Fn is due to the fact that the wetted surface of the model is altered to some extent by the generated wave system.

2.2 Wave making resistance.

The wave making resistance of a ship is related to the net force upon the ship due to the normal fluid pressures acting on the hull, just as the frictional resistance is the result of the tangential fluid forces. If the body is travelling on or near the free surface this pressure variation causes waves which radiate away from the body and carry with them a certain amount of energy that is dissipated in the ocean. The wave making resistance can then be also characterized by the energy expended by the ship that is necessary to maintain the wave system. Theoretical determination of the wave making resistance requires knowledge of the wave system generated by a moving ship.

The first serious theoretical attempt towards quantifying the ship wave system was due to Lord Kelvin in the late 19th century. He considered a single pressure point travelling in a straight line over the surface of the water, sending out waves which combine to form a characteristic pattern. This consists of a system of transverse waves following behind the point, together with a series of divergent waves radiating from the point, the whole pattern being predominantly contained within two straight lines starting from the pressure point and making angles of about 19 degrees on each side of the line of motion, see Figure 7. The Kelvin wave pattern illustrates and explains many of the features of the ship wave system. The whole wave pattern moves with the ship, and for an observer on the ship the waves appear to be stationary. Although at first it may seem that replacing the ship by a single pressure point is too simplified, it should be borne in mind that this is a far field approximation valid far away from the body where the geometric characteristics of the hull are not visible. Kelvin was able to arrive at his model using a general technique in asymptotic

analysis, called the method of stationary phase, which he developed precisely for the wave resistance problem. The method allows the approximate evaluation of certain integrals of rapidly oscillating functions and it produces two wave systems: One that is inside the 19 deg cusp lines of Figure 7, and one that is outside. The interior waves dissipate as $O(1/\sqrt{R})$ where R is the radial distance from the ship; whereas the exterior as $O(1/R)$ and, therefore, they can be neglected for large R .

The method of stationary phase predicts for the wave making resistance R_w

$$R_w = \frac{1}{2}\pi\rho V^2 \int_{-\pi/2}^{\pi/2} |A(\theta)|^2 \cos^3 \theta d\theta . \quad (28)$$

Equation (28) expresses the wave resistance of a moving vessel as the weighted integral of the square of the wave amplitude $A(\theta)$. The factor $\cos^3 \theta$ implies that the dominant portion of the resistance will be associated with the transverse waves where the angle θ is smaller. We can see that $R_w \sim V^2 A^2$, and since $A \sim V$ (at least), it follows that $R_w \sim V^4$ (or higher). Now since the frictional resistance increases like V^2 or less (why?) we can see that at high speeds (or high Fn) the wave making resistance will dominate the total ship resistance and will create a practical “barrier” — compare the various hull types shown in Figure 2.

To utilize equation (28), the wave amplitude $A(\theta)$ must be predicted from theory (a rather difficult task) or measured in a suitable experiment. One way of evaluating $A(\theta)$ is based on the thin ship theory which was introduced by Michell in 1898 as a purely analytic approach for predicting the wave resistance of ships. The essential assumption is that the hull is thin, that is, the beam is small compared to all other characteristic lengths of the problem. The resulting solution can be expressed in terms of a distribution of sources and sinks on the centerplane of the hull, with the local source strength proportional to the longitudinal slope of the hull. This solution is analogous to the thickness problem of thin wing theory in aerodynamics. The result is the so called Mitchell’s integral

$$R_w = \frac{4g^2}{\pi V^2} \int_0^{\pi/2} \sec^3 \theta \left| \iint \frac{\partial \zeta}{\partial x} \exp[(g/V^2) \sec^2 \theta (y - ix \cos \theta)] dx dy \right|^2 d\theta , \quad (29)$$

where $\zeta(x, y)$ defines the local half-beam of the hull surface. This multiple integral is not the sort of expression one expects to find in a table of integrals, particularly since in practical cases the longitudinal slope of the ship hull cannot be expressed in terms of simple mathematical functions. Nevertheless, a fairly large number of numerical computations have been carried out both for practical ship geometries and for simplified mathematical forms. Mitchell’s integral is an effective means of comparisons between different theoretical predictions or different hull forms.

More recent numerical studies of wave making resistance do away with the thin ship assumption and follow the so called panel methods. In these the surface of the ship is approximated by a series of panels with distributed sources and sinks. The method is similar to the thin ship approximation with the difference that the source/sink distribution is on the actual ship surface instead of the centerplane. This allows for the actual geometry of the hull to be taken into account, and therefore, minor modifications can be inflicted in order to minimize the wave making resistance, for example appropriate bulbous bow design. An example of such detailed computations is shown in Figure 8 where the wave contours

generated by a DDG-51 similar hull at $F_n=0.28$ are shown. It can be seen that the basic features of the elementary Kelvin system (divergent and transverse waves) are evident, along with more detailed characteristics such as the bow and shoulder waves.

The use of the wave resistance integral (28) with experimental measurements of the amplitude function $A(\theta)$ to determine the total wave resistance provides a direct measurement of the wave resistance without recourse to Froude's hypothesis. This approach is known as wave pattern analysis. The wave pattern analysis requires a relatively complex survey of the wake region to determine the amplitude function $A(\theta)$ for all relevant wave angles, and it is a valuable diagnostic tool, particularly when used with a measurement of the momentum defect in the viscous wake region. These techniques have led to the discovery of an additional drag component associated with *wave breaking*, and to a better understanding of the bulbous bows of supertankers and other ships with low Froude numbers.

In fine high speed vessels such as destroyers and passenger liners, a bulbous bow promotes beneficial interference between the waves generated at different points along the length of the hull. Thus, for such vessels, the bulb bow reduces the wave making resistance. Originally, bulbous bows of a similar form were fitted to supertankers on the basis of experimental measurements indicating significant reductions in the total drag, but these reductions often exceed the total estimated wave resistance. This apparent paradox has been reconciled by careful experimental measurements of the wave energy flux and of the momentum defect in the wake due to the viscous form drag. The latter measurement has revealed the existence of momentum associated with breaking waves. Thus the wave breaking resistance results from the breaking of waves near the ship, predominantly at the bow. The energy lost in this manner is convected downstream in the form of large scale turbulence or eddies. For supertankers and similar vessels, the bulbous bow is effective in reducing the magnitude of the bow wave and thereby in avoiding wave breaking. For naval vessels, this is particularly interesting since it is related to non acoustic signature and detection considerations.

A typical plot of the wave breaking resistance coefficient versus Froude number is shown in Figure 9, where the curve shows typical humps and hollows. These are attributed to the interference effects which are due to the four major wave systems, generated at

- the bow, beginning with a crest;
- the forward shoulder, starting with a trough;
- the after shoulder, starting with a trough;
- the stern, beginning with a crest.

A comparison between calculated and measured wave making resistance coefficient is also presented in Figure 9. Experimental results are usually obtained by wake survey techniques outlined above. In general, there is good agreement, although the computed C_W curves show more oscillations than the experimental results. These differences are assigned to three major causes:

1. Errors due to simplifications introduced to the mathematical analysis.
2. Errors due to neglect of the effects of viscosity on the wave making resistance.

3. Errors due to the effects of wave motion on the frictional resistance.

At very low speeds the wave making resistance is very small and depends mainly on the waterline shape at the bow (angle of entrance), whereas at very high speeds it varies approximately as the square of the displacement. This illustrates the fact that at very high speeds hull shape is relatively unimportant, the chief consideration being the displacement carried on a given length.

2.3 Other components of resistance.

Besides the frictional and wave making resistance, it was pointed out before that several other components contribute to the resistance of a ship such as eddy resistance, viscous pressure drag, separation resistance, and wave breaking resistance.

The turbulent frictional belt around a ship consists of eddies or vortices, so that all forms of frictional resistance are really due to eddy making. However, the term is usually applied to the resistance due to eddy formation or disturbed streamline flow caused by abrupt changes of form, appendages or other projections, and excludes tangential skin friction. When the total model resistance R_{TM} is measured over a range of speeds and plotted as the coefficient $C_{TM} = R_{TM}/\frac{1}{2}\rho SV^2$ against $\log Re$ (R_n in the figure), the curve will be of the general shape shown in Figure 10. Also shown is a curve of the coefficient of frictional resistance C_{FOM} for a smooth flat plate in fully turbulent flow. The intercept C_{RM} between the curves of C_{FOM} for the flat plate and C_{TM} for the total model resistance is the so called residuary resistance coefficient. In a typical case the C_{TM} curve at the very low values of Re is almost parallel to the C_{FOM} curve but some distance above it. Since the primary component of the coefficient C_{WM} varies roughly as the fourth power of the speed, the wave making resistance at very low values of Re must be vanishingly small, and so the intercept C_{RM} (BC in Figure 10) cannot be attributed to this cause. If a curve is drawn parallel to the curve of C_{FOM} , the intercept FG represents the wave making resistance coefficient $C_{WM} = R_{WM}/\frac{1}{2}\rho SV^2$. On this assumption, the intercept FE (=BC) must be due to some other cause, and this is the *form* resistance.

There are three main causes of this form resistance. The ordinate of the C_{FOM} curve applies to a flat surface having the same length and wetted area as the model and so neglects any effects due to the curvature of the hull. This curvature affects the pressure distribution along the length, causing the velocity to increase along most of the middle part and to decrease at the ends. The former effect outweighs the latter. Also, since the path along a streamline from bow to stern is longer on a shaped body than on a flat plate, the average velocity must be higher. Thus, the real skin friction of a ship must be greater than that of the equivalent flat plate. Since the pressure and velocity changes and the extra path lengths are greater the fuller and stumper the form, such shapes would be expected to have greater form drag. This has been verified by experiments on bodies of revolution run deeply submerged. For a given volume of displacement, increases in the length to diameter ratio L/D beyond a certain point, while it may still reduce the form drag, will increase the frictional resistance because of the greater surface area and so in terms of total resistance there will be some optimum value of the L/D ratio. The value depends on the exact shape and on the amount of appendages necessary to provide directional stability and control, and varies between 5

and 7. For surface ships the intercept C_{RM} has been found to vary from 5 to 15 percent of C_{FOM} in naval vessels and up to 40% or more in full cargo ships. These increases, however, cannot be attributed solely to curvature effects, which leads to the other causes of form effect.

The existence of the boundary layer has the virtual effect of lengthening the form and reducing the slopes of the after waterlines. This is a region where the normal pressure on the hull is higher than the static pressure and the forward components of these excess pressures will exert a forward thrust overcoming some of the ship's resistance. The presence of the boundary layer reduces these forward components, resulting in an increase in resistance as compared with that which would be experienced in a nonviscous fluid, and is called the *viscous pressure drag*.

If the curvature near the stern becomes too abrupt, the water may no longer be able to follow the hull and breaks away, and the space between the hull and the smooth flowing water is filled with vortices, as illustrated in Figure 1. A point at which this happens is called a separation point, and the resulting resistance is the third element of form drag, called separation resistance. Separation of this kind can also affect the pressure distribution on the hull, and so modify the viscous pressure drag. In addition to form and separation resistance, eddy making resistance is also caused by struts, shafts, bossings and other appendages.

Especially in the case of bluff hull forms the phenomena of *wave breaking* and wave breaking resistance have to be considered as well. For this type of hull the flow ahead of the bow becomes irregular and complex, usually leading to a breaking wave, mentioned in the previous section as well. At very low Froude numbers, below approximately 0.10, wave making hardly occurs and the free surface at the stern rises to a height approximately equal to $V^2/2g$, where V is the speed of the ship and g the acceleration due to gravity, in accordance with Bernoulli's equation. As the ship speed increases however, this rise of the wave at the stern no longer occurs and instead the bow wave breaks. The resistance associated with wave breaking has been the subject of extensive investigations. Bow wave breaking is considered to be due to flow separation at the free surface, and it can generally be avoided by requiring that the tangent to the curve of sectional areas at the forward perpendicular be not too steep. At a certain ship speed the free surface becomes unstable and breaks when the radius of curvature of the curved streamlines results in a value of the centrifugal acceleration V^2/R greater than a critical value. This is the so called Taylor instability criterion (1950), and when applied to the case of the flow around the bow of a ship with radius R , results in the approximate expression that $R \geq V^2/50$, with R in meters and V in m/sec, to avoid wave breaking.

1. Wind resistance.

A ship sailing on a smooth sea and in still air experiences air resistance but this is usually negligible, and it may become appreciable only in high wind. Although the wind speed and direction are never constant and considerable fluctuations can be expected in a storm, constant speed and direction are usually assumed. Even in a steady wind the speed of the wind varies with height above the sea. For consistency therefore the speed is quoted at a datum height of 10 m. Near the sea surface the wind is considerably slower than at and above the datum height. According to Davenport the variation of speed with height can be

sufficiently represented by

$$\frac{W_z}{W} = \left(\frac{z}{z_g} \right)^{1/n},$$

where z_g is the datum height, W is the mean wind speed at the datum height, and n is about 7.5 for the atmosphere (this is like the 7–th power law in turbulent boundary layers).

The axial wind force (wind resistance) is given in terms of a coefficient C_{XA} which is expressed as

$$C_{XA}(\psi_A) = \frac{\text{Axial force at relative wind angle } \psi_A}{1/2\rho_A A_{TA} W^2},$$

where A_{TA} is the transverse projected area of the ship. The axial wind force coefficient C_{XA} is function of the relative wind angle ψ_A and typically it varies between ± 0.8 as ψ_A varies from 0 to 180 degrees. The above force is generally insignificant except when the ship is “stopped” in a wind or during low speed maneuvering. The wind side force is computed on the basis of the lateral (side) projected area A_{LA} , and is given by the expression

$$C_{YA}(\psi_A) = \frac{\text{Side force at relative wind angle } \psi_A}{1/2\rho_A A_{LA} W^2}.$$

The variation of C_{YA} with the relative wind angle is generally more or less sinusoidal, and the maximum value of about 0.8 occurs near 90 degrees (beam wind). The yaw moment generated by the wind is

$$C_{NA}(\psi_A) = \frac{\text{Moment at relative wind angle } \psi_A}{1/2\rho_A A_{LA} L_{OA} W^2},$$

where L_{OA} is the length overall and the moment coefficient is

$$C_{NA}(\psi_A) = x_A(\psi_A) C_{YA}(\psi_A),$$

where x_A is the center of pressure, which typically varies between ± 0.3 of the ship’s length.

2. Added resistance due to waves.

Winds are seldom encountered at sea without wind-generated waves, sometimes from distant storms. Such waves approaching the ship from ahead can cause appreciable added resistance, in part from the diffraction effect of the moving hull on the encountered waves and partly from the indirect effect of the heaving and pitching motions caused by the waves. In beam and quartering seas, there may be heavy rolling and some yawing, both of which will add to the resistance. Required rudder action, in particular during tight maneuvers, may also make a significant addition. Discussion of these effects will be delayed until Part IV.

3. Appendage resistance.

The principal appendages in ships are the bilge keels, rudders, bossings or open shafts and struts. All these items give rise to additional resistance, which is best determined by model experiments. For rudders this can also be calculated from a knowledge of their shape, using

drag coefficients for airfoils of similar characteristics and Reynolds numbers appropriate to their speed and length. The correlation of model measurements to the ship is a difficult question which is not yet satisfactorily solved. The model appendages themselves are very small, so that the Reynolds numbers based upon their speed and dimensions are also small, and scale effect is likely to be important. This is especially so with struts and open shafts. Some tanks have adopted the practice of measuring the increase in C_{TM} on the model due to appendages, and adding only half of this to the total bare hull ship resistance coefficient. Other tanks make no such reduction, adding the full value of the increase in C_{TM} to the ship bare hull resistance, so that the designer must be aware of the specific towing tank techniques. As a means of making approximate estimates of appendage resistance for design purposes, table 1 quotes overall figures derived from model tests, no reduction being made for scale effects. The appendage resistance is expressed as percent of bare hull resistance.

4. Trim effects.

Due to the change in pressure distribution around a ship at different speeds, it will rise or sink and trim. At low speeds there is a general sinkage and a slight trim by the bow as compared with the at rest condition, Figure 11. As speed increases the movement of the bow is reversed and at about $Fn = 0.30$ the bow begins to rise appreciably, the stern sinks still further and the ship takes on a decided trim by the stern, Figure 11.

In the average merchant ship form, additional trim by the stern in the at rest condition usually results in an increase in resistance at low speeds and a decrease at high speeds. At low speeds the increased draft aft makes the stern virtually fuller, with a consequent increase in form and separation resistance, whereas at high speeds this is more than offset by the reduction in wave making due to the finer entrance in the trimmed condition.

In ballast condition it is usually necessary to carry considerable trim by the stern in order to ensure adequate immersion of the propeller, and this will have similar effects to those stated in the foregoing — higher resistance at low speeds, less at high speeds. For any ship which is likely to spend an appreciable part of her time at sea in ballast condition, model experiments are usually made to investigate these effects.

5. Shallow water effects.

The resistance of a ship is quite sensitive to the effects of shallow water. In the first place there is an appreciable change in potential flow around the hull. If the ship is considered as being at rest in a flowing stream of restricted depth, but unrestricted width, the water passing below it must speed up more than in deep water, with a consequent greater reduction in pressure and increased sinkage, trim usually by the stern, and resistance. If in addition the water is restricted laterally, as in a river or canal, these effects are further exaggerated. The sinkage and trim in very shallow water may set an upper limit to the speed at which ships can operate without touching bottom.

A second effect is the changes in the wave pattern which occur in passing from deep to shallow water. When the water is very deep, the wave pattern consists of the Kelvin transverse and diverging waves shown in Figure 7, the pattern being contained between the straight lines making an angle α of 19 deg 28 min on each side of the line of motion. As is discussed more fully in Part IV and in Fluid Mechanics courses, the velocity of surface waves

is

$$V_c^2 = \frac{g\ell_w}{2\pi},$$

in deep water where ℓ_w is the wave length, and

$$V_c^2 = gh,$$

in shallow water where h is the water depth. The wave pattern for a moving pressure point goes through a critical change when $V = \sqrt{gh}$, see Figure 12. For speeds less than $V = \sqrt{gh}$, the system consists of a double set of waves, transverse and diverging as in deep water, advancing with the pressure point at velocity V . For values of V less than about $0.4\sqrt{gh}$, the pattern is enclosed between the straight lines having an angle $\alpha = 19$ deg 28 min to the centerline, as for deep water. As V increases above this value, the angle α increases and approaches 90 deg as V approaches \sqrt{gh} . All the wave making effect is now concentrated in a single crest through the pressure point and at right angles to its direction of motion, the wave being called a wave of translation. When V exceeds \sqrt{gh} , the angle α begins to decrease again, the wave system being contained between the lines given by $\sin \alpha = \sqrt{gh}/V$. It now consists only of diverging waves, there being no transverse waves or cusps. The two straight lines themselves are the front crests of the diverging system, and the inner crests are concave to the line of advance instead of convex as in deep water.

The resistance effect due to these changes is shown in Figure 13 for a pressure disturbance of linear dimension l travelling over water of depth h . It can be seen from the figure that the peaks occur at about $V \approx \sqrt{gh}$, the critical speed for that particular water depth. At this speed the resistance is much greater than in deep water, but ultimately at a sufficiently high speed it becomes less than in deep water. This depth effect has an important bearing on full scale ship trials, and can cause misleading results on the relation between power and speed.

Speeds below and above $V = \sqrt{gh}$ are referred to as subcritical and supercritical, respectively. Nearly all displacement ships operate in the subcritical zone, the exceptions being fast naval ships. The ship speed loss

$$\delta V = V_\infty - V_h,$$

where V_∞ is the speed at deep water, and V_h at water depth h , expressed in percentage terms as $100 \times \delta V/V_\infty$, is shown in Figure 14 where A_x is the maximum cross sectional area of the hull.

When the ship is operating in shallow water *and* in restricted channels, the corresponding speed loss can be evaluated from Figure 15 where R_H denotes the hydraulic radius of the channel defined as

$$R_H = \frac{\text{area of cross section of channel}}{\text{wetted perimeter}}.$$

For a rectangular channel of width b and depth h

$$R_H = \frac{bh}{b + 2h}.$$

When b becomes very large, $R_H = h$, and this corresponds to the previous case of shallow water of unrestricted width. When a ship or model is in a rectangular channel, the hydraulic radius is

$$R_H = \frac{bh - A_x}{b + 2h + p},$$

where A_x is the maximum cross sectional area of the hull, and p the wetted girth of the hull at this section.

6. Subsurface waves.

Another wave phenomenon which illustrates several features of pressure resistance due to wavemaking even more forcibly than waves generated at an air–water interface is that associated with the so called “dead water”. A layer of fresh water often rests on a layer of salt water, with little or no mixing, as in regions of rapidly melting ice or off the mouths of large volume fresh water rivers or fiords. A slow ship or a tug and tow moving through the low density upper layer may be greatly retarded and rendered almost unmanageable, because of the generation of low velocity internal waves at the fresh–salt water interface. Indeed, under these circumstances the internal or subsurface waves have a vertical height or amplitude much greater than that of the surface waves, yet they are rarely, if ever, detectable from above the free surface.

The augmented resistance due to these waves can be risen to two or three times the wave making resistance in homogeneous water. It is also significant to note that for the subsurface waves:

- Wavemaking at the submerged interface is not necessarily accompanied by wavemaking at the free surface.
- Wavemaking at a submerged interface can be set up by a body or ship floating on and in an upper layer of liquid, when the body does not project into the lower layer.

If the ratio of densities of fresh and salt water is represented by s , then the speed of propagation of the subsurface waves compared to the speed of free surface waves is diminished in the ratio $[(1 - s)/(1 + s)]^{0.5}$, and for fresh over salt water $s = 0.9662$ and the ratio is 0.131. This reduces the speed of the subsurface waves significantly so that if the ship speed is above 5 kts, there is little chance that the ship will be caught by dead water.

2.4 Relation of hull form to resistance.

In research problems concerned with the separation of resistance into its components, methods of extrapolation to the ship, model–ship correlation allowance and the like, the total resistance coefficient

$$C_T = \frac{R_T}{0.5\rho SV^2},$$

is usually used, plotted to a base of the logarithm of Reynolds number $Rn = VL/\nu$. Curves of this kind have been used in earlier sections. In any consistent system of units, both C_T and Rn are dimensionless.

For design purposes, a method is desired which will show the relative merits of different ship forms. Ships are usually designed to carry a given displacement at a specified speed. C_T is not suitable for such cases, since it is based on wetted surface and not on displacement, and can lead to misleading presentations. An obvious merit criterion is the resistance per unit displacement weight, R_T/W , which is nondimensional when R_T and W are expressed in the same units. This ratio is the basis of a number of presentations, which differ principally with regards to the speed coefficient used as the base.

Since lower resistance implies lower fuel costs, minimization of ship resistance is clearly a consideration in the design spiral. A new ship is usually required to carry a certain deadweight at a particular speed, and the designer then estimates the probable displacement and principal dimensions. The latter are usually subject to restrictions not associated with resistance and propulsion. Length is expensive in first cost, is limited by docking and navigation restrictions, while added length increases scantlings, equipment and manning scales. From a resistance point of view, greater length for a given displacement will reduce the wave making resistance but increase the frictional resistance, so that longer lengths will be beneficial in ships running at high speeds and vice-versa. Longer lengths are also generally beneficial for behavior in rough seas.

An increase in draft, T , is generally beneficial for resistance, and is a cheap dimension in terms of cost. However, it may be limited by depths of harbors, canals, or rivers.

The beam, B , is one of the governing factors in ensuring adequate stability, and a minimum value of B/T is generally necessary on this account. An increase in B will increase the resistance unless it is accompanied by a corresponding finer hull. In cases of low speed ships however, a small reduction in length and a compensating increase in beam, because of the resulting decrease in wetted surface, may result in little or no increase in resistance. This results in a cheaper ship and also meets the need for increased stability in ships with large superstructures. This idea has been exploited in a number of large tankers.

The minimum wetted surface for a given displacement is also sensitive to the B/T ratio, the optimum value of which is about 2.25 for a block coefficient of 0.80 and about 3.0 at 0.50. However, the penalty for normal departures from these values is not very great. The effects of changes in B/T on wave making resistance can be studied from model experiment results. Generally, stability considerations and limiting drafts usually preclude values below 2.25 for full ships and 2.5 or even more for fine, higher speed hull forms.

While such considerations may be of guidance to naval architects in the choice of dimensions, they must meet many other demands, and will be influenced to a large extent by their knowledge of the particulars of existing successful ships. The process of design is essentially an iterative one, in which the various elements are changed until a proper balance is attained. In order to do this, parametric surveys have to be made on the effects of changes in dimensions, hull form, machinery types, and coefficients of form.

An approximate relation between the block coefficient C_B and the Froude number F_n can be expressed by

$$\frac{V}{\sqrt{gL}} = 0.595(1.08 - C_B) ,$$

for trial speed, and

$$\frac{V}{\sqrt{gL}} = 0.595(1.05 - C_B) ,$$

for service speed. A similar formula for the sustained sea speed in terms of the prismatic coefficient C_P , is

$$\frac{V_S}{\sqrt{gL}} = 0.55 - 0.48C_P ,$$

where the trial speed is taken as

$$V_T = 1.06V_S .$$

The above relationships are intended as rough guides to the designer and do not take the place of a careful analysis, model experiments, and comparison of alternative designs. Relations between speed length ratio V/\sqrt{L} (V in knots, L in feet), prismatic coefficient C_P , and displacement length ratio $W/(0.01L)^3$ (W in tons, L in feet) are shown in Figure 16. The underwater volume of the hull is denoted by ∇ , so that there is no confusion with the speed V . The curves of this figure are based upon data from a variety of sources, and result in two pairs of empirical curves which define two “design lanes”. These apply to merchant and combatant vessels of customary form, and not to special types such as fishing vessels and tugs.

The load waterplane coefficient C_{WP} decreases with increasing fullness, its value depending also to a considerable extent upon the type of transverse sections. For Series 60 it is related to the C_P by the approximate formula

$$C_{WP} = 0.18 + 0.86C_P .$$

In general, C_{WP} will depend also on stability requirements and seakeeping.

In full ships considerable parallel body can be worked in with advantage, and the entrance can be short, the run being long and fine to minimize flow separation and form resistance. As C_P decreases, so does parallel body, and the entrance is made longer to reduce the increase in wave making resistance, the LCB moving aft in consequence. Most of the reduction in C_P is thus accomplished by fining the entrance, the change in the coefficient of the run being much less.

In designing a new ship, systematic series of data for comparisons among a number of choices of hull form and proportions are available in the technical literature. Such a well known standard series is the Taylor series developed by Admiral Taylor in the 1930’s in DTRC (Experimental Model Basin, EMB, at the time). The original parent hull was patterned after a British cruiser with the scary name *Leviathan*. The sectional area curves and body lines for the other models were derived from the parent partly by mathematical means. The lines of the parent form are shown in Figure 17. The midship section coefficient was 0.925. The prismatic coefficients of the fore and aft bodies were equal, and the LCB was always amidships. The quantities varied were C_P , B/T , and $W/(L/100)^3$, the midship section coefficient C_M remaining constant. The ranges of the variables covered in the Taylor standard series are (dimensionless or British units):

$$\begin{aligned} C_P &= 0.48 \text{ to } 0.86, \\ B/T &= 2.25, 3.00, \text{ and } 3.75, \\ W/(L/100)^3 &= 20 \text{ to } 250, \\ \nabla/L^3 &= 0.70 \text{ to } 8.75 \times 10^{-3}. \end{aligned}$$

The design charts give contours of the residual resistance coefficient C_R against V/\sqrt{gL} for various values of ∇/L^3 , each chart being for a particular value of C_P and B/T , and a typical set is shown in Figure 18. In conjunction with frictional resistance coefficients (Figure 5) and an appropriate allowance coefficient (page 99), they can be used to provide design estimates of the total ship resistance. In using the Taylor series results it should be borne in mind that the models have a deep cruiser stern suitable for a twin screw propulsion arrangement. Also the LCB location has not been optimized but is stationed at amidships.

Other systematic ship resistance series include the following:

(a) Series 60: Very popular series developed by the Society of Naval Architects and Marine Engineers in cooperation with the ATTC. It is based on a single screw merchant parent and includes data on LCB variations, trim effects, and some propulsive data. It has a narrower range than Taylor series. Many other results have been developed for this series.

(b) BSRA Series: This has resulted from a long series of tests with single screw merchant type hulls. It was developed by the British Ship Research Association in the 1960's. A comparison between Taylor, Series 60, and BSRA is shown in Table 2.

Here $C_\Delta = W/(0.01L)^3$ and L_p is the length of the parallel midbody as percent of the length between perpendiculars. The terms in the last row are propulsion related factors and they will be examined in the next section.

(c) SSPA Series: Developed by the Swedish State Shipbuilding Experimental Tank in the 1950's and includes data for high speed, twin screw cargo liners; fast, single screw cargo ship models; tankers; and single screw cargo ships.

(d) NPL Series: Developed by the National Physical Laboratory, England, it contains data for coaster models and high speed displacement crafts.

(e) Formdata Series: Developed in Denmark fairly recently (in the 1970's), it is an attempt to combine the previous main series, Taylor, 60, SSPA, and NPL.

3. Ship Propulsion.

Propulsive devices for ships may take many forms but in the following sections only mechanical means of propulsion will be discussed. Of the mechanical means the screw propeller has been found most use and this section will be devoted exclusively to this. Before actually discussing propeller theory and design it is important to understand the terms used, and also to have some knowledge of certain principles of hydrodynamics.

3.1 Powering of ships.

We can begin by defining the basic power terms, as schematically depicted in Figure 19. The *brake power*, P_B , is the power measured at the crank-shaft coupling by means of a mechanical, hydraulic, or electrical brake. It is determined by a shop test and is calculated by the formula

$$P_B = 2\pi Qn \text{ in kW ,}$$

where

$$Q = \text{brake torque, kN-m}$$

n = revolutions per sec.

The brake power is commonly used in internal combustion engines. In terms of horsepower we have $1 \text{ hp} = 0.7457 \text{ kW}$, where $1 \text{ hp} = 550 \text{ ft-lb per sec}$.

The *shaft power*, P_S , is the power transmitted through the shaft. It is usually measured aboard the ship by means of a torsionmeter. This instrument measures the angle of twist between two sections of the shaft, which angle is directly proportional to the torque transmitted. Usually we write

$$P_S = P_B \eta_G , \quad (30)$$

where η_G is the gearing efficiency. Through the bearing efficiency η_B and the sterntube efficiency η_S , we arrive at the *delivered power*

$$P_D = P_B \eta_S \eta_B \eta_G , \quad (31)$$

which is the power available to the propeller for the propulsion of the ship.

As the propeller advances through the water at a speed of advance V_A , it delivers a thrust T , and the *thrust power* is

$$P_T = TV_A . \quad (32)$$

Now the ship moves with speed V and experiences resistance R , so that the *effective power* is

$$P_E = RV . \quad (33)$$

This is related to P_D through the quasi-propulsive efficiency

$$\eta_D = \frac{P_E}{P_D} . \quad (34)$$

The coefficient η_D is in the range of 0.5 to 0.7 whereas all other efficiencies are very close to 1.

In order to facilitate our notation, in the following the product $\eta_S \eta_B \eta_G$ will be simply termed η_S , the shaft transmission efficiency. The *propulsive efficiency* is then defined by

$$\eta_P = \frac{P_E}{P_B} = \eta_D \eta_S . \quad (35)$$

Finally, the ratio of the work done on the ship to that done by the propeller is called the hull efficiency

$$\eta_H = \frac{P_E}{P_T} = \frac{RV}{TV_A} . \quad (36)$$

3.2 Propeller action.

Early attempts to explain the mechanism which is used by the propeller to drive the ship focused around the momentum theory. In this the propeller is regarded as a “disk” capable of imparting an increase of pressure or acceleration to the fluid passing through it, the mechanism by which it does so being in the background. Momentum theories are based

on correct fundamental principles, but give no indication of the propeller form which would produce the required thrust.

More recent progress follows the circulation theory. In its simplest form, this yields the blade element theory of propeller action, where the propeller is considered to be made up of a number of separate blades, which in turn can be divided into successive strips across the blades, from leading to trailing edge, Figure 20. The forces acting on each strip can be evaluated from a knowledge of the relative velocity of the strip to the water and the geometry of the section shape. The elementary forces are then resolved into the elements of thrust dT in the forward direction, and of torque dQ in the plane of propeller rotation. By plotting curves of dT and dQ along the blade from boss to tip, as in Figure 20, curves of thrust and torque loading are obtained which when integrated will give the total thrust T and torque Q on the whole propeller. The propeller efficiency is then defined by

$$\eta_0 = \frac{TV_A}{2\pi nQ} . \quad (37)$$

The shapes of blade outlines and sections vary significantly according to the type of ship for which the propeller is intended. Figure 21 shows a typical design and defines many of the terms in common use.

If we consider a section of the propeller blade at a radius r with a pitch angle ϕ and pitch P , and imagining the blade to be working in an unyielding medium, then in one revolution of the propeller it will advance from A to A' , a distance called the *pitch*, P . If we unroll the cylinder of radius r into a flat surface, the helix traced out by A will develop into a straight line AM , and the angle

$$\tan \phi = \frac{P}{2\pi r} ,$$

is the *pitch angle*. If the screw is turning at n revolutions per unit time, then in that time it will advance a distance Pn and we can obtain a velocity diagram for the section as in Figure 21. In a real fluid, there will be a certain amount of yielding when the propeller is developing thrust and the screw will not advance a distance LM , equal to Pn , in unit time, but some smaller distance LS , the distance MS being called the *slip*. The ratio $MS/ML = s_R$ is called the *real slip ratio* and MAS the slip angle or geometrical slip angle. From Figure 21, it can be seen that

$$s_R = \frac{Pn - V_A}{Pn} = 1 - \frac{V_A}{Pn} . \quad (38)$$

3.3 Law of similitude for propellers.

As in the case of resistance, a great deal of knowledge concerning the performance of propellers can be gained from experiments on models and it is important therefore to examine the relation between model and full scale results. Dimensional analysis can be used to establish this relation and in what follows an expression will be obtained for the thrust produced by a propeller.

The thrust of the propeller, T , could depend upon:

1. Mass density of water, ρ .

2. Propeller size, represented by the diameter, D .
3. Speed of advance, V_A .
4. Acceleration due to gravity, g .
5. Speed of rotation, n .
6. Pressure in the field, p .
7. Viscosity of the water, μ .

Writing

$$T = f(\rho^a D^b V_A^c g^d n^e p^f \mu^g),$$

and introducing the proper dimensions we have

$$\frac{ML}{T^2} = \left(\frac{M}{L^3}\right)^a (L)^b \left(\frac{L}{T}\right)^c \left(\frac{L}{T^2}\right)^d \left(\frac{1}{T}\right)^e \left(\frac{M}{LT^2}\right)^f \left(\frac{M}{LT}\right)^g. \quad (39)$$

Equating the indices of M , L , and T on the two sides of equation (39) leads to

$$\frac{T}{\frac{1}{2}\rho D^2 V_A^2} = f\left(\frac{gD}{V_A^2}, \frac{nD}{V_A}, \frac{p}{\rho V_A^2}, \frac{\nu}{V_A D}\right), \quad (40)$$

where $\nu = \mu/\rho$. Equation (40) states that if all parameters on the right hand side have the same values for two geometrically similar but different size propellers, the flow patterns will be similar and the value of $T/\frac{1}{2}\rho D^2 V_A^2$ will be the same for both.

If the model and ship quantities are distinguished by the subscripts M and S , respectively, and if λ is the linear scale ratio, then

$$\frac{D_S}{D_M} = \lambda.$$

If the model propeller is run at the correct Froude speed of advance, then also

$$\frac{V_{AS}}{V_{AM}} = \lambda^{1/2}.$$

Under these circumstances, the first term gD/V_A^2 in equation (40) will be the same for model and ship, so that the first condition for dynamic similarity is that the speed of advance of the model and ship propellers should be in accordance with Froude scaling.

The slip ratio has been defined by equation (38). For geometrically similar propellers, therefore, the second condition of equation (40) that nD/V_A must be the same for model and ship, means that the slip ratio must be kept the same for both. Just as in the case of ship resistance, the third quantity in equation (40) cannot be the same for model and ship propellers when the former is run in a towing tank, because the atmospheric pressure is not scaled down in the latter case. However, since the forces on the propeller blades are caused by differences in pressure, they will not be affected by this fact unless cavitation occurs, in which case other kinds of tests must be made (see Section 3.5). The last term, $\nu/V_A D$, is a

Reynolds number, and it cannot be made the same if the model and ship speeds of advance follow Froude's law. It is concerned with the frictional resistance on the propeller blades, but as this is only a very small part of the total force on the blade, we can neglect the effects of viscosity. Nevertheless, it is necessary to make the model propeller as large as feasible in order to reduce such Reynolds number effects on the blade section drag to a minimum.

With these in mind, we can say that as long as gD/V_A^2 and nD/V_A are the same in ship and model

$$T \propto D^2 V_A^2 .$$

The following relationships also hold:

$$\begin{aligned} \frac{D_S}{D_M} &= \lambda , & \frac{V_{AS}}{V_{AM}} &= \lambda^{1/2} , \\ \frac{T_S}{T_M} &= \frac{D_S^2 V_{AS}^2}{D_M^2 V_{AM}^2} = \lambda^3 , \\ \frac{n_S D_S}{V_{AS}} &= \frac{n_M D_M}{V_{AM}} , \end{aligned}$$

or

$$\frac{n_S}{n_M} = \frac{D_M V_{AS}}{D_S V_{AM}} = \lambda^{-1/2} \quad \text{or} \quad n_M = n_S \lambda^{1/2} ,$$

i.e., the model revolutions are higher than those on the full scale propeller.

The thrust power is given by $P_T = TV_A$, so that

$$\frac{P_{TS}}{P_{TM}} = \frac{T_S V_{AS}}{T_M V_{AM}} = \lambda^{3.5} ,$$

and

$$\frac{Q_S}{Q_M} = \frac{P_{TS}}{n_S} \cdot \frac{n_M}{P_{TM}} = \lambda^4 .$$

If the model results were plotted as values of

$$C_T = \frac{T}{\frac{1}{2} \rho D^2 V_A^2} ,$$

and

$$C_Q = \frac{T}{\frac{1}{2} \rho D^3 V_A^2} ,$$

to a base of $J = V_A/nD$, therefore, the values would be directly applicable to the ship, apart from any scale effects. This method of presentation is often used, but the coefficients have the disadvantage that they become infinite for zero speed of advance, a condition sometimes occurring in practice, such as for a tug pulling at a stationary ship.

Since $J = V_A/nD$ is the same for model and ship, we can replace V_A by nD and obtain new coefficients which do not have this disadvantage:

$$\text{Advance ratio, } J = \frac{V_A}{nD} ; \tag{41}$$

$$\text{Thrust coefficient, } K_T = \frac{T}{\rho n^2 D^4}; \quad (42)$$

$$\text{Torque coefficient, } K_Q = \frac{Q}{\rho n^2 D^5}; \quad (43)$$

$$\text{Open water propeller efficiency, } \eta_0 = \frac{J}{2\pi} \cdot \frac{K_T}{K_Q}; \quad (44)$$

where K_T , K_Q , and η_0 are functions of J . These coefficients are dimensionless in any consistent system of units.

Typical open water propeller curves are shown in Figure 22. These show that this propeller reaches its maximum efficiency at a J -value of about 0.85. Since $P/D = 1$ for this propeller, at $J = 1$ the slip ratio is $s_R = 0$ (so why isn't the thrust zero there?).

3.4 Hull propeller interaction.

In the previous discussion, the propeller was assumed to be working in undisturbed or open water. When it is located behind the model or ship hull, the flow is considerably modified. The propeller is now working in water which has been disturbed by the passage of the hull, and in general the water around the stern has acquired a forward motion in the same direction as the ship. This forward moving water is called the wake, and one of the results is that the propeller is no longer advancing relatively to the water at the same speed as the ship, V , but at some lower speed V_A , called the *speed of advance*. The relations between thrust, torque, and revolutions in open water where the inflow is uniform, cannot be expected to remain the same behind the hull in the variable flow conditions experienced there. This leads to the possibility of different propeller efficiencies in open water and behind the hull.

1. Wake. The difference between the ship speed V and the speed of advance V_A is the wake speed. The *wake fraction* is defined as

$$w = \frac{V - V_A}{V}, \quad (45)$$

and then $V_A = V(1 - w)$. The wake is due to three principal causes:

(a) The frictional drag of the hull causes a following current which increases in velocity and volume towards the stern, and produces there a wake having a considerable forward velocity relative to the surrounding water.

(b) The streamline flow past the hull causes an increased pressure around the stern, where the streamlines are closing in. This means that in this region the relative velocity of the water past the hull will be less than the ship's speed and will appear as a forward or positive wake augmenting that due to friction.

(c) The ship forms a wave pattern on the surface of the water, and the water particles in the crests have a forward velocity due to their orbital motion, while in the troughs the orbital velocity is sternward. This orbital velocity will give rise to a wake component which will be positive or negative according to whether there is a crest or a trough of the wave system in the vicinity of the propeller.

The total wake is made up of these three components, and in the great majority of cases is positive, with the exception of high speed ships. The wake has other significant effects

on the behavior of the ship, predominantly propeller induced hull vibrations discussed in Section 2.5 of Part II.

2. Slip Ratio. The real slip ratio has been defined, equation (38), as

$$s_R = 1 - \frac{V_A}{Pn} .$$

For the propeller working behind the hull, another slip ratio can be calculated using the ship speed V instead of the speed of advance of the propeller. This is called the *apparent slip ratio*, s_A , given by

$$s_A = 1 - \frac{V}{Pn} . \quad (46)$$

The real slip ratio is the only real guide to the ship's performance and requires a knowledge of the wake fraction, w . However, the apparent slip ratio, which needs only the values of ship speed, revolutions, and propeller pitch for its calculation, is often recorded in ships' log books.

3. Relative Rotating Efficiency. The propeller in open water, with a uniform inflow velocity at a speed of advance V_A , has an *open water efficiency* given by

$$\eta_0 = \frac{TV_A}{2\pi nQ_0} , \quad (47)$$

where Q_0 is the torque measured in open water when the propeller is delivering thrust T at n rotations. Behind the hull, at the same effective speed of advance V_A , the thrust T and revolutions n will be associated with some different torque Q , and the *efficiency behind the hull* will be

$$\eta_B = \frac{TV_A}{2\pi nQ} . \quad (48)$$

The ratio of behind to open efficiencies under these conditions is called the *relative rotative efficiency*, being given by

$$\eta_R = \frac{\eta_B}{\eta_0} = \frac{Q_0}{Q} . \quad (49)$$

The difference in torque found behind and in open is due to two main reasons: the heterogeneous wake, and the fact that the amount of turbulence in the water behind the hull is greater than in open water. The value of the relative rotative efficiency does not in general depart significantly from one, being in the range of 0.95 to 1.0 for most twin screw ships, and between 1.0 and 1.1 for single screw.

4. Thrust Deduction. When a hull is towed, there is an area of high pressure over the stern which has a resultant forward component reducing the total resistance. With a self propelled hull, however, the pressure over some of this area is reduced by the action of the propeller in accelerating the water flowing into it, the forward component is reduced, the resistance is increased and so is the thrust necessary to propel the model or ship. If R is the resistance and T the thrust, we can write for the same ship speed

$$R = (1 - t)T , \quad (50)$$

where the expression $(1 - t)$ is called the *thrust deduction factor*.

5. Hull Efficiency. The work done in moving a ship at a speed V against a resistance R is proportional to the product RV or the effective power P_E . The work done by the propeller in delivering a thrust T at a speed of advance V_A is proportional to the product TV_A or the thrust power P_T . The ratio of the work done on the ship by that done by the propeller is called the *hull efficiency*, η_H , so that

$$\eta_H = \frac{P_E}{P_T} = \frac{RV}{TV_A} = \frac{1-t}{1-w}. \quad (51)$$

For most ships this is greater than one. At first sight this seems an anomalous situation in that apparently something is being obtained for nothing. It can, however, be explained by the fact that the propeller is making use of the energy which is already in the wake because of its forward velocity.

6. Propulsive Efficiency. In equation (34) the quasi-propulsive efficiency was defined as

$$\eta_D = \frac{\text{effective power}}{\text{delivered power}} = \frac{P_E}{P_D},$$

where

$$\begin{aligned} P_E &= RV, \quad \text{and} \\ P_D &= \frac{TV_A}{\eta_B}, \end{aligned}$$

from equation (48). Therefore,

$$\eta_D = \frac{RV}{TV_A} \eta_B,$$

and from the relationships already developed, this can be expanded into the form

$$\begin{aligned} \eta_D &= \frac{1-t}{1-w} \eta_B = \frac{1-t}{1-w} \cdot \frac{\eta_B}{\eta_0} \eta_0 \\ &= \frac{1-t}{1-w} \eta_R \eta_0 = \eta_H \eta_R \eta_0. \end{aligned} \quad (52)$$

The overall propulsive efficiency is then given from (35) as

$$\eta_P = \eta_H \eta_R \eta_0 \eta_S. \quad (53)$$

The division of the propulsive coefficient into factors in this way is of great assistance both in understanding the propulsion problem and in making estimates of propulsive efficiency for design purposes.

3.5 Cavitation.

Cavitation is a phenomenon met with in highly loaded propellers in which, beyond certain critical revolutions, there is a progressive breakdown in the flow and a consequent loss of thrust. In its extreme form, it may prevent the ship from reaching the desired speed. Before this stage is reached, however, it manifests itself by noise, vibration and erosion of the

propeller blades, struts, and rudders. Avoidance of cavitation has become an important requirement in the design of nearly all propellers, and it is necessary to consider the problem of cavitation before going on to methods of propeller design and selection.

To understand the mechanism of cavitation, consider a blade section or airfoil set at a small angle of attack in a two dimensional, steady, nonviscous flow, Figure 23. On this diagram a horizontal line is drawn which represents the static pressure on the back of the blade. If the reduction in pressure on the back should equal the static pressure at any point in the breadth of the blade then any tendency to reduce the pressure beyond this point will cause flow breakdown and the formation of cavities filled with air or water vapor. Now these cavities or bubbles will be swept along the blade and as they move towards the trailing edge they will come into regions of higher pressure and collapse. The collapse of the bubbles generates very highly localized forces, sufficient to cause mechanical damage to the material of the blade, or erosion. For quantitative purposes, it is necessary to have some criterion which will indicate the conditions under which a propeller is working as far as cavitation is concerned.

With reference to Figure 23, Bernoulli's equation yields

$$p_1 + \frac{1}{2}\rho V_1^2 = p_0 + \frac{1}{2}\rho V_0^2 ,$$

and the change in pressure is

$$\delta p = p_1 - p_0 = \frac{1}{2}(\rho V_0^2 - \rho V_1^2) .$$

At some point S near the leading edge of the section, the velocity V_1 is zero. This point S is called a stagnation point and the pressure at S , called the stagnation pressure, is

$$q = \frac{1}{2}\rho V_0^2 .$$

The pressure p_1 at some point on the back of the blade will become zero if

$$\delta p = -p_0 .$$

Since water cannot support tension, the flow will break down at this point with the formation of bubbles and cavities, and cavitation will result. In practice, this situation will come about somewhat earlier — when p_1 has fallen not to zero but to the vapor pressure of water, p_v , at which it begins to “boil” and form cavities. The criterion is then that

$$\begin{aligned} p_v &= p_0 + \delta p , \quad \text{or} \\ \delta p &= -(p_0 - p_v) . \end{aligned}$$

Dividing through by the stagnation pressure $\frac{1}{2}\rho V_0^2$ or q , cavitation will begin when

$$-\frac{\delta p}{\rho} \geq \frac{p_0 - p_v}{q} .$$

The expression

$$\frac{p_0 - p_v}{q} = \sigma , \tag{54}$$

is called the *cavitation number*.

In model experiments, the dimensional analysis of Section 3.3, revealed that for dynamic similarity the term $p/\rho V_A^2$ must remain the same for model and full scale propeller — refer to equation (40). It can be seen that this is equivalent to saying that the cavitation number σ must be the same. In order to establish the cavitation characteristics of a propeller, therefore, the tests must be run at the same value of σ , while still keeping Froude scaling. Such tests are done in cavitation tunnels or variable pressure towing tanks where the pressure can be reduced to the correct scale amount.

Many propellers, especially during an initial design phase, are designed from charts derived from methodical series tests, as presented in Section 3.6. Even if they are designed by using analytical tools, it is still necessary to begin with some chosen propeller diameter, also determined from a design chart. Some general criterion is therefore needed for the choice of blade area to avoid cavitation. A diagram designed to provide such guidance in order to avoid excessive cavitation and erosion under average service conditions at sea was given by Burrill and is presented in Figure 24. In the diagram, the local cavitation number $\sigma_{0.7R}$ is calculated using the relative speed V_R at 0.7 radius and the pressure at the centerline of the propeller, i.e.,

$$\sigma_{0.7R} = \frac{p_A - p_v + \rho gh}{\frac{1}{2}\rho [V_A^2 + (0.7\pi nD)^2]},$$

an approximate value for which is

$$\sigma_{0.7R} = \frac{188.2 + 19.62h}{V_A^2 + 4.836n^2D^2}, \quad (55)$$

where h is the head of water at the propeller center line (m), D the propeller diameter (m), n revolutions per second, and V_A the speed of advance (m/sec). On the vertical scale of the diagram, a coefficient τ_c expressing the mean thrust loading on the blades, is defined

$$\tau_c = \frac{T/A_P}{\frac{1}{2}\rho V_R^2},$$

where T is the thrust in kN, A_P the projected blade area in m^2 , and V_R is given by $V_R^2 = V_A^2 + (0.7\pi nD)^2$. A suggested limit on T/A_P can then be obtained in order to avoid serious back cavitation. The projected blade area A_P can be found from the more usual developed area A_D by using Taylor's approximate formula (refer to Figure 21 for the definitions)

$$\frac{A_P}{A_D} = 1.067 - 0.229\frac{P}{D}. \quad (56)$$

We remind that the thrust can be calculated from the effective power P_E or the delivered power P_D from the expressions

$$T = \frac{P_E}{(1-t)V} = \frac{P_D\eta_D}{(1-t)V}.$$

A useful formula for obtaining a first indication as to the required expanded blade area ratio was derived by Keller

$$\frac{A_E}{A_0} = \frac{(1.3 + 0.3Z)T}{(p_0 - p_v)D^2} + k, \quad (57)$$

where T is the thrust, Z the number of propeller blades, $p_o - p_v$ the pressure at the centerline of the propeller, k is a constant varying from 0 (for transom stern naval vessels) to 0.20 (for high powered single screw vessels), A_0 is the propeller disk area $\pi D^2/4$, and A_E is the expanded blade area derived from the expanded blade outline as shown in Figure 21.

The subject of cavitation criteria in propeller design can really only be dealt with adequately by incorporating pressure distribution, angle of attack, and cavitation number information into a detailed design process, for every radius. Criteria such as the Burrill chart and the Keller formula do not reflect the influence of the wake or propeller blade geometry such as pitch, camber, and thickness distribution. They should, therefore, be used with care for preliminary estimates only.

3.6 Propeller selection and design.

The design of a marine propeller can be carried out either by purely theoretical calculations or by using charts and methodical series, in which case it is more propeller selection than design. In this section we concentrate our efforts more on propeller selection and less on design, the latter being a very complicated problem.

1. General considerations in propeller design.

Propeller efficiency usually increases with increasing *diameter*, D , and the maximum diameter is limited by the geometry of the stern. Another limiting factor is imposed by propeller induced unsteady hull forces which decrease with increasing hull/propeller clearance. Also a larger diameter will change the radial distribution of the wake in which the propeller operates, which can lead to serious detrimental effects if the blades extend into a region of greater flow non-uniformity.

The *number of revolutions*, n , is in many cases selected beforehand and may not be a part of the final design. In general, a reduction in rpm tends to be beneficial.

The *number of blades*, Z , affects predominantly the level of the unsteady forces on the propeller. The main consideration that influences the selection of Z is to avoid hull resonance, as was briefly discussed in Section 2.5 of Part II.

The *expanded blade area*, A_E , is generally selected to avoid cavitation. This can be done by using, for example, equation (57).

Finally, with a view to the recent developments of highly skewed propellers, it is appropriate to mention their properties. Properly designed skewed propellers have the following advantages:

- Decrease in propeller induced unsteady bearing forces and moments.
- Decrease in propeller induced unsteady pressure forces.
- Decreased susceptibility to cavitation when operating in a wake.

These advantages are at the expense of:

- Decreased backing efficiency.
- More difficult to manufacture.

- Strength related problems for very high skew and for backing conditions.

Appropriate skew design can be achieved only with detailed analytical studies and it requires a fairly accurate knowledge of the wake in which the propeller will be operating.

2. Propeller selection from methodical series.

In conducting model propeller series tests, a parent model is chosen of given blade area, number of blades, blade outline, section shape, and blade thickness, and a number of models are built with different pitch ratios. These models are then run in open water in a towing tank over a range of slip ratios. Additional groups can be run in which one of the other parameters is changed and the effect of the alteration on performance determined. The most widely used systematic propeller series is the Wageningen B-series. The range of Z and A_E/A_0 that the series covers is shown in Table 3.

Any particular group of series B is identified by combinations such as B.5.60 where 5 indicates the number of blades and 0.60 the expanded blade area ratio. A typical form of a four blade propeller is shown in Figure 25.

The open water propeller characteristics are presented in graphical form in terms of the thrust and torque coefficients

$$K_T = \frac{T}{\rho n^2 D^4}, \quad K_Q = \frac{Q}{\rho n^2 D^5}, \quad (58)$$

and the open water propeller efficiency

$$\eta_0 = \frac{J}{2\pi} \cdot \frac{K_T}{K_Q}, \quad (59)$$

versus the advance coefficient

$$J = \frac{V_A}{nD}, \quad (60)$$

and for different values of the pitch ratio P/D . A typical propeller chart is shown in Figure 26. Each diagram is for a certain value of Z and A_E/A_0 , which are selected based on the previous general considerations.

In the propeller selection problem we have the two equations (58) and six basic unknowns: T (or R), V_A (or V), P , D , n , and Q . Therefore, if we know four of these unknowns we can solve the problem and select the propeller. As an example, suppose we know the ship resistance R at the required service speed V from the resistance calculations of the previous sections. We have already selected a type of main engine and the revolutions n are known. We know the propeller diameter D , and we want to find the pitch P and the delivered power P_D . In order to do this we have to estimate t and w and, therefore, we know T , V_A , n , and D . From these we can find K_T and J from equations (58) and (60), and this defines a point on the K_T - J diagram. The curve P/D that passes through that point determines the pitch, and the corresponding value of K_Q yields the open water torque Q at the propeller. The delivered power is then

$$P_D = \frac{2\pi n Q_0}{\eta_R}. \quad (61)$$

If three instead of four of the parameters are known, and a relationship between two of the remaining, for instance R or P_E versus V , we have to solve an optimization problem. The optimality criterion is normally the propeller efficiency (59). During preliminary design we usually have two main categories of such propeller optimization problems:

Optimal revolution: We know V , P_E or R , and D (for example, the largest propeller that fits under the stern), and we want to find P and n to maximize η_0 . The solution procedure is as follows: Estimate t and w and compute T and V_A . Therefore, we can compute the ratio

$$\frac{K_T}{J^2} = \frac{T}{\rho V_A^2 D^2} = C_1 . \quad (62)$$

The curve $K_T = C_1 J^2$ is then plotted on the K_T - J diagram. This curve corresponds to the ship requirements, Figure 27. The intersection of this curve with any one of the K_T - J curves constitutes a potential solution to the problem, and we can find the corresponding efficiency η_0 . If this procedure is performed for all K_T - J curves in the diagram, we can plot the curve η_0 - J and the maximum of this curve corresponds to the optimal propeller.

If, instead of P_E , the delivered power P_D is known, we have

$$K_Q = \frac{Q}{\rho n^2 D^5} = \frac{P_D \eta_R}{2\pi \rho n^3 D^5} ,$$

and we can see that the ratio K_Q/J^3 is now constant. By superimposing this curve on the propeller chart, we can construct the η_0 - J curve and determine the optimal propeller.

Optimal diameter: Suppose that V , P_E , and n are given — for example, we know what kind of main engine and gearing is to be installed, but we don't know the engine horsepower. We need to determine the propeller diameter D and pitch P for maximum efficiency η_0 . Similarly to the previous case we can see that here the ratio

$$\frac{K_T}{J^4} = \frac{T n^2}{\rho V_A^2} ,$$

is known. The selection procedure is then similar to the optimal revolution case. If P_D instead of P_E is given, we can see that the ratio K_Q/J^5 will now be known and the rest of the procedure is the same.

The above procedures can also be performed numerically by using some standard optimization technique, such as the Lagrange multiplier method. This is possible because the curves K_T and K_Q are also given in polynomial form for the Wageningen B-series in terms of the parameters J , P/D , A_E/A_0 , and Z . All these curves apply for Reynolds number 2×10^6 . Corrections for different Reynolds numbers exist but they are rather insignificant. The results are usually given in tables or graphical form.

At the final design stage now we have decided on the particular main propulsion unit to be installed on the ship. This introduces one more level of complexity since the propeller characteristics must match the main engine characteristics as closely as possible. A typical engine power vs. engine speed diagram for a Sulzer 2-stroke engine is shown in Figure 28. It is desirable that the propeller characteristics curve is located in region A and must go through point *M.C.R.*, or close to it. Each point on such a curve corresponds to a different propeller/engine operation point and can be parametrized by the specific fuel consumption

and the ship speed. From such detailed diagrams it is possible to evaluate how successful the final design is. If, for example, the propeller operates at full speed with little power, it has too small a pitch ratio. If, on the other hand, it operates at full power at low speed, its pitch is too high. The advantages and added flexibility of a controllable pitch propeller become now evident — such topics will be covered through homework problems.

3. Theoretical propeller design.

The use of a design method based upon a rational theory permits the designer the ability to account for the following:

- number of blades
- hub size
- radial blade loading
- chordwise blade loading
- blade shape and size
- blade skew
- wake adaption

All of these features, with the possible exception of hub size, can play a major role in minimizing ship vibration and/or cavitation problems. The proper recognition of propeller blade strength requirements can only be achieved within the framework of a theoretical design method.

Figure 29 presents a schematic diagram of the propeller design process. The first two steps involve recognition of the available data, design constraints, selection of design parameters, and initial estimates. These ensure that the propeller will be compatible with the ship, installed propulsion machinery, and transmission from the standpoint of efficiency and vibration.

Step III involves the use of a *lifting line* program. This allows for computation of the optimum spanwise lift distribution over the propeller blade, the hydrodynamic pitch angle, the inflow velocity to each blade section, the total thrust which is produced, the power which is absorbed, and the propeller efficiency. Lifting line theory cannot account for chordwise effects but can recognize spanwise (radial) effects. The main hypotheses and assumptions of the lifting line concept can be summarized as follows:

1. The fluid is inviscid and incompressible. However, in the calculation procedure, allowance is made for the viscous drag of the blade by the use of some kind of strip theory.
2. The free stream velocity is axisymmetric and steady.
3. Each propeller blade is represented by a lifting line and the circulation varies along the radius. From vortex theory it follows that free vortices are shed from the lifting line and, in a coordinate system that rotates with the propeller, these free vortices form a general helical surface behind the propeller.

4. Each of the free vortices is at a constant pitch in the downstream direction, but a radial variation in pitch is allowed. This means that effects of centrifugal force on the shape of the vortex sheets are ignored.
5. The radial velocity induced at the hub is assumed small so that the effect of the hub on the pitch of the trailing sheets is ignored.

The lifting line results allow detailed cavitation and strength analysis. The preliminary estimates of thickness and chord distribution made in Step II can now, in Step IV, be checked and altered if necessary. It might be found that the optimum load distribution found in Step III cannot be achieved. In particular, the tip might have to be unloaded. In this case, a non-optimum load distribution will have to be developed and the lifting line program re-run.

Step V involves skew and rake selection. Both are very important in controlling propeller excited vibrations. Vibration excitation results from both the unsteady pressure forces acting on the hull and the unsteady bearing forces which result from the varying loading on the propeller. Blade rake is used to increase the distance between the propeller and the hull. Blade skew permits a more gradual entry of the blade into the high wake region. Thus, both rake and skew tend to reduce the propeller excitation forces.

Lifting line theory cannot recognize chordwise effects and thus it is not sufficient to use two dimensional section data to obtain the required angle of attack and camber for relatively broad bladed marine propellers. To obtain the chordwise effects, we must use a *lifting surface* program, Step VI, to compute the lifting surface corrections for the angle of attack and camber distributions. The previous lifting line theory assumptions hold for lifting surface, except now it is assumed that the bound vortices are distributed over the blade surface rather than concentrated at a lifting line, and the blade is allowed to have a finite thickness.

The lifting surface program can predict the loading and velocity distribution over the entire propeller blade. These can be used for a final cavitation check, Step VII. In addition, the loading can be put into a finite element program to conduct a detailed structural analysis.

LIST OF FIGURES

	Page
1. Examples of flow about a submerged body.	91
2. Speed–power trends for different ship types.	93
3. Velocity profiles for the boundary layer on a flat plate.	98
4. Skin friction lines, turbulent and laminar flow.	99
5. Standard skin friction lines.	100
6. Ship resistance calculation using Hughes form factor method.	101
7. Kelvin wave pattern.	103
8. Ship generated waves prediction.	105
9. Typical wave making resistance coefficient plots.	107
10. Elements of model resistance.	108
11. Changes in sinkage and trim with speed.	112
12. Effect of shallow water on wave pattern.	113
13. Effect of shallow water on wave resistance.	114
14. Chart for calculating reduction in speed in shallow water.	114
15. Curves for calculating resistance in restricted channels.	115
16. Design lanes for prismatic coefficient and displacement length ratio.	118
17. Lines for the parent form of Taylor standard series.	119
18. Typical Taylor standard series contours.	120
19. Ship power definitions.	122
20. Propeller blade definitions and loading curves.	123
21. Typical propeller drawing and definitions.	124
22. Typical K_T , K_Q , and η_0 curves.	128
23. Flow and pressure around an airfoil.	132
24. Burrill’s cavitation diagram.	134
25. Blade form and sections of B.4 series.	136
26. Wageningen B–series propeller: $Z = 4$, $A_E/A_0 = 0.9$, $P/D = 0.5$ to 1.4 .	137
27. Example of optimal revolution propeller selection.	138
28. Typical main engine and propeller characteristics.	141
29. Theoretical propeller design steps.	142

LIST OF TABLES

	Page
1. Appendage resistance for various ship types.	91
2. Range of applicability of resistance standard series.	93
3. Range of applicability of B-series propellers.	

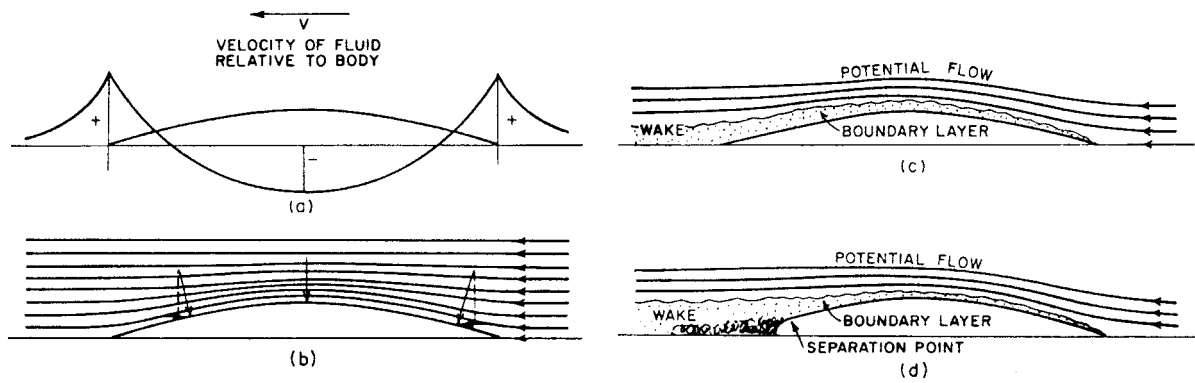


Figure 1: Examples of flow about a submerged body.

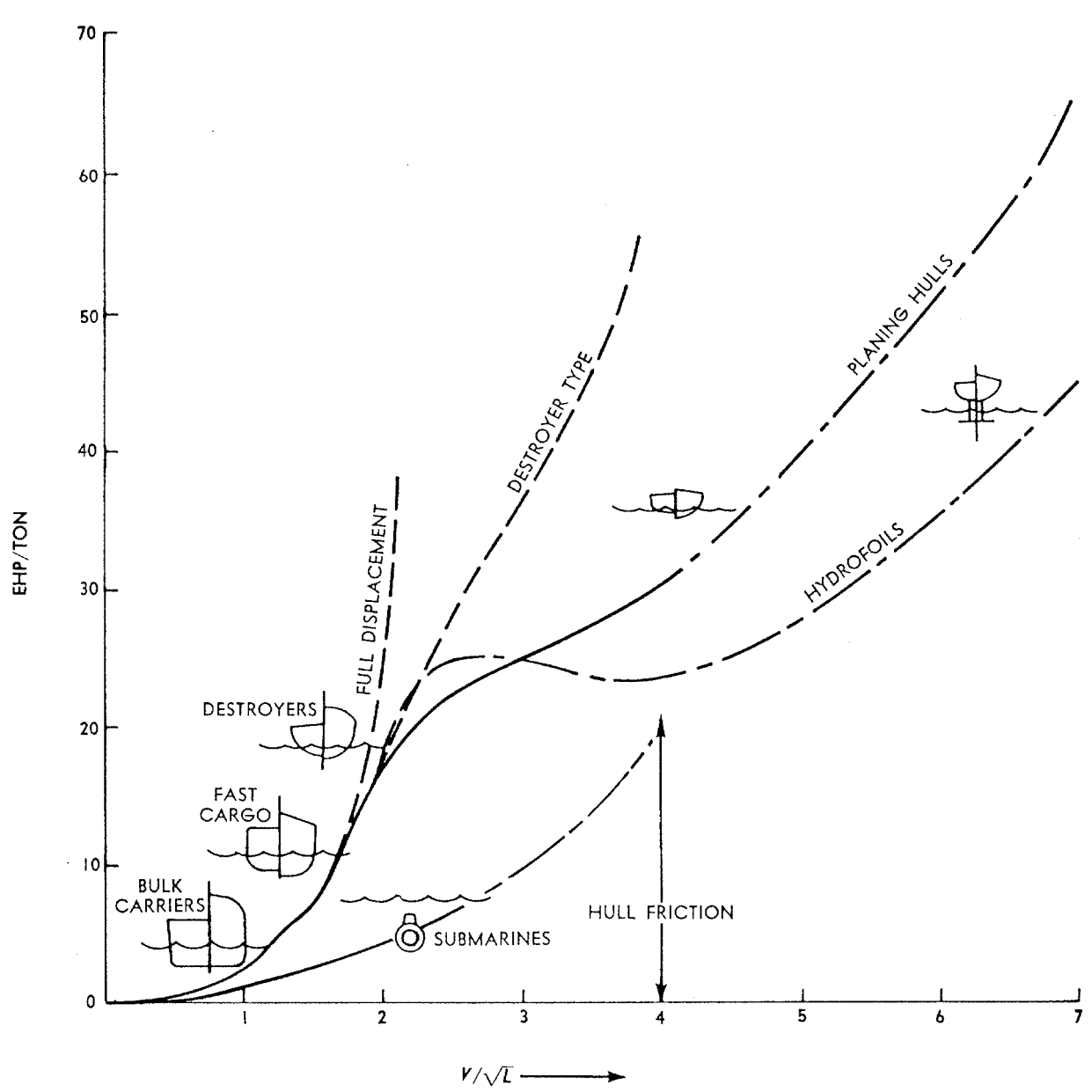
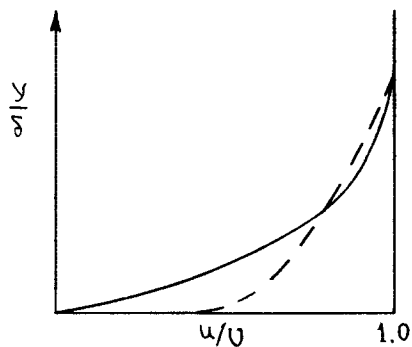


Figure 2: Speed–power trends for different ship types.



Comparison of laminar (—) and mean turbulent (---) sketches of velocity profiles, for the boundary layer on a flat plate. Since the boundary layer thickness is substantially greater in the turbulent case, the difference in scales should be noted in this comparison.

Figure 3: Velocity profiles for the boundary layer on a flat plate.

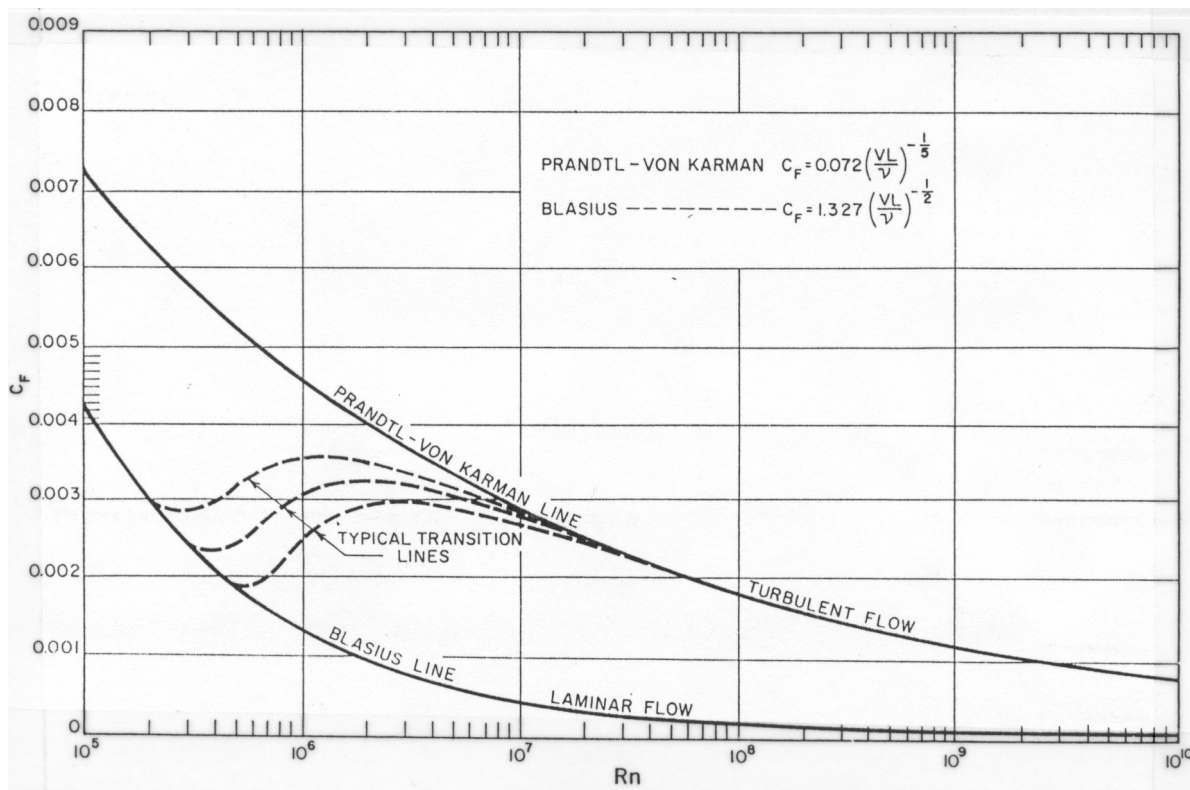


Figure 4: Skin friction lines, turbulent and laminar flow.

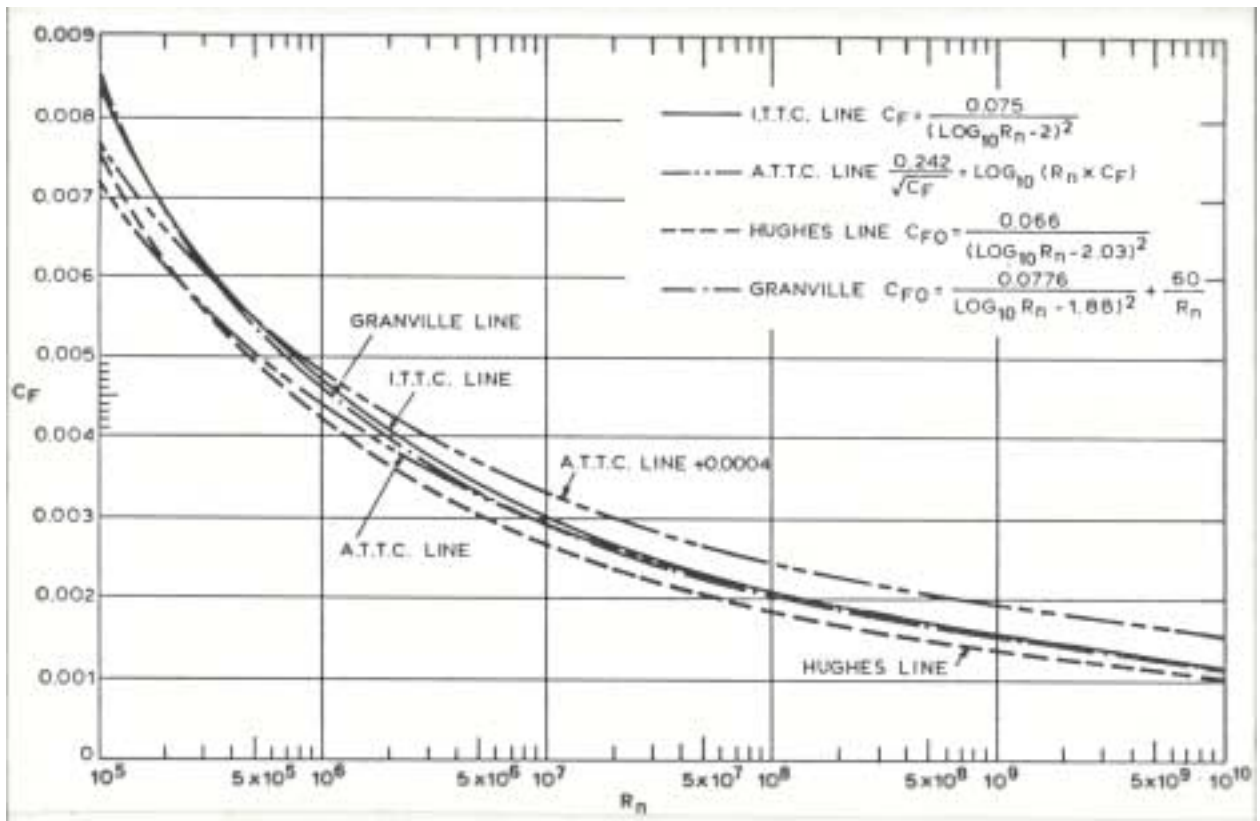


Figure 5: Standard skin friction lines.

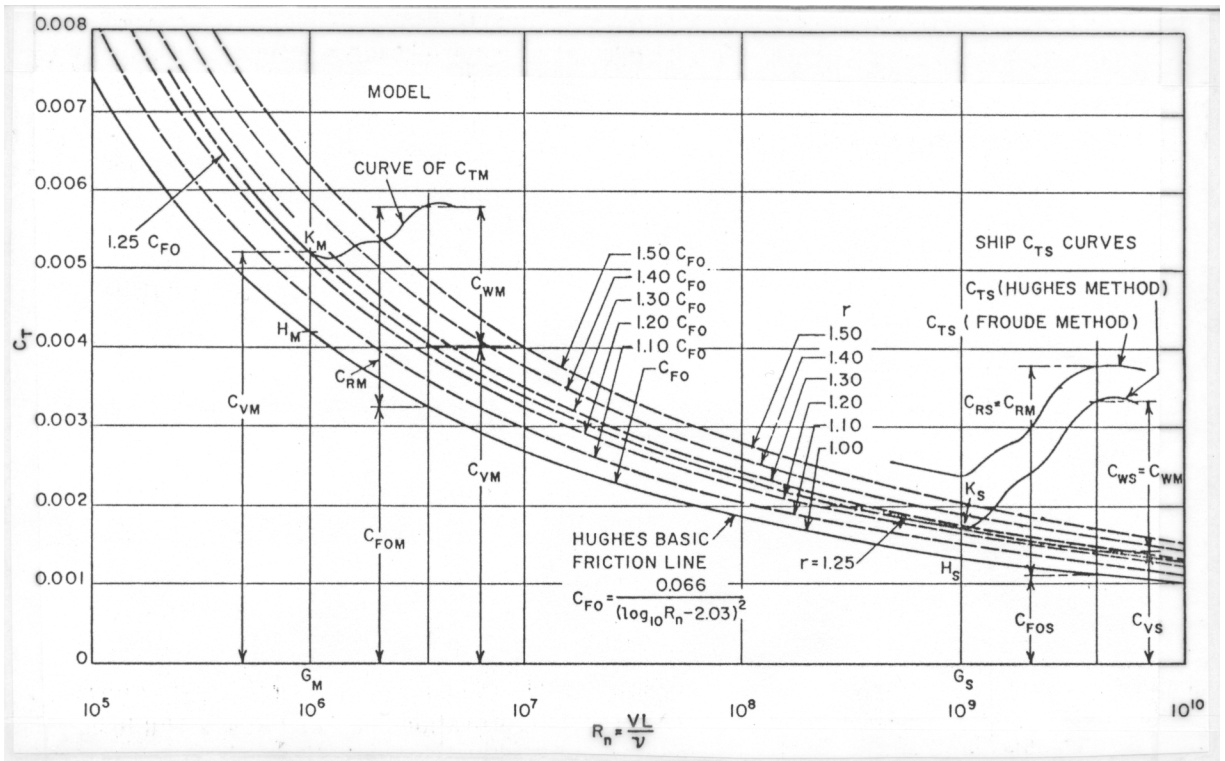


Figure 6: Ship resistance calculation using Hughes form factor method.

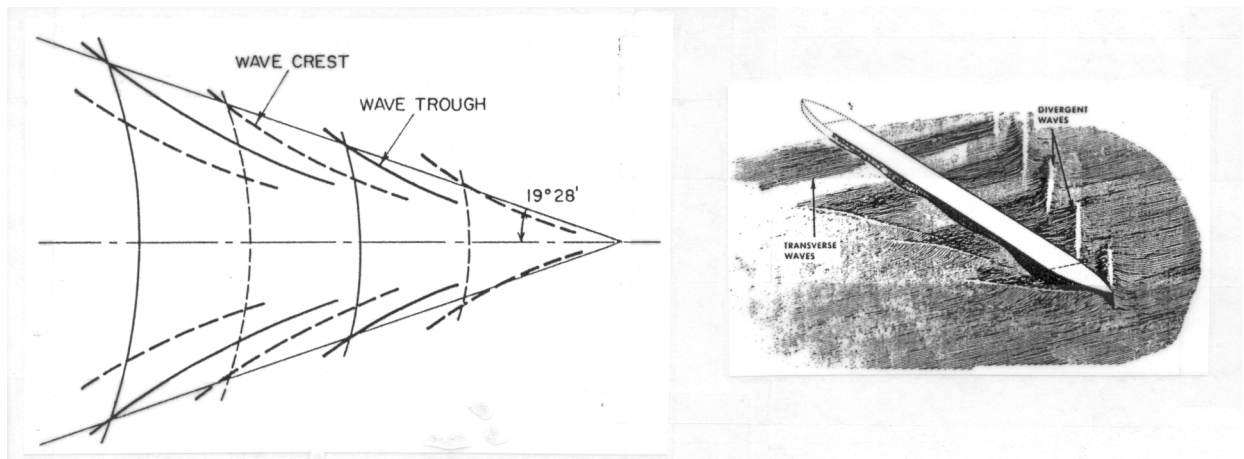


Figure 7: Kelvin wave pattern.

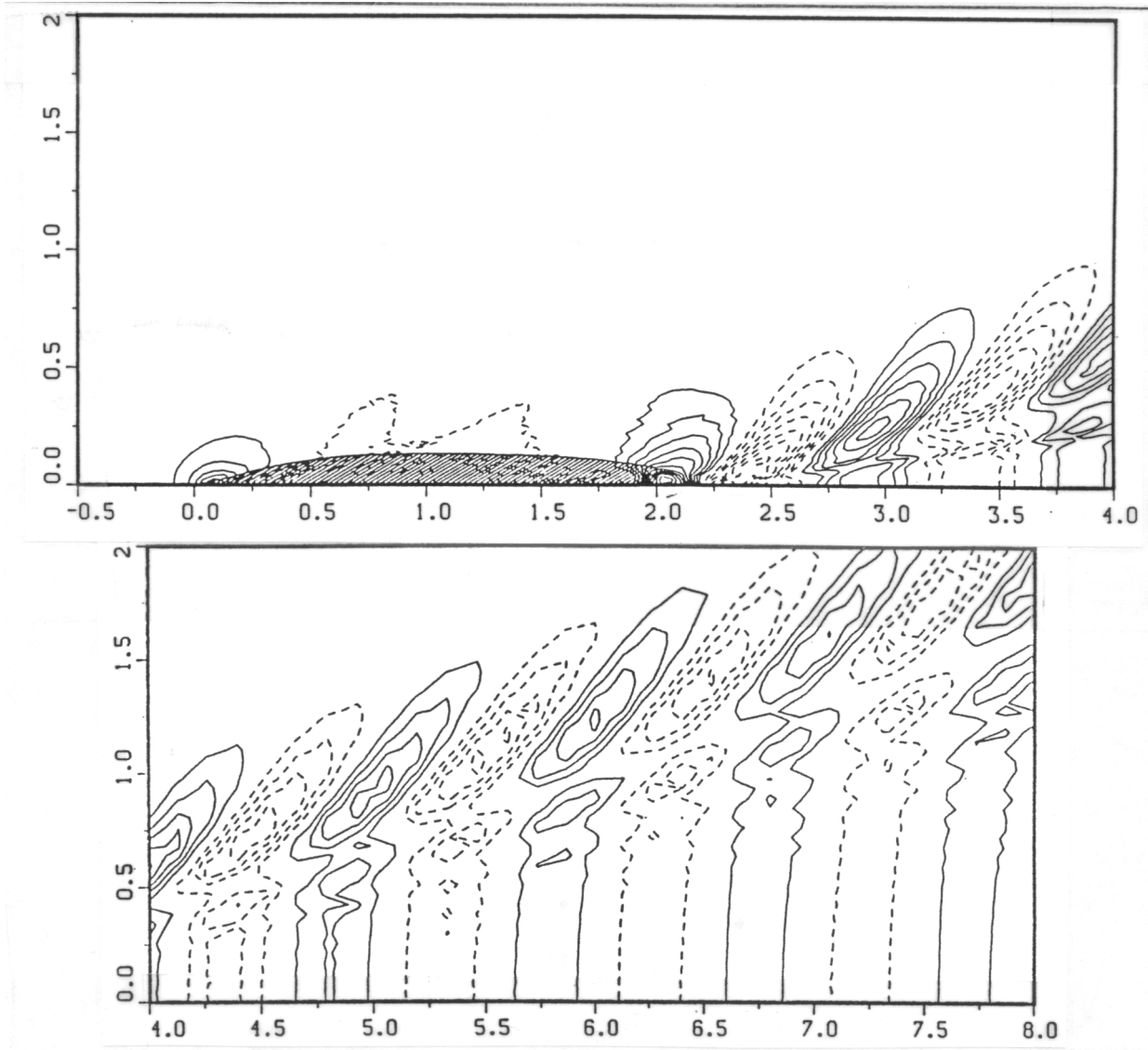


Figure 8: Ship generated waves prediction.

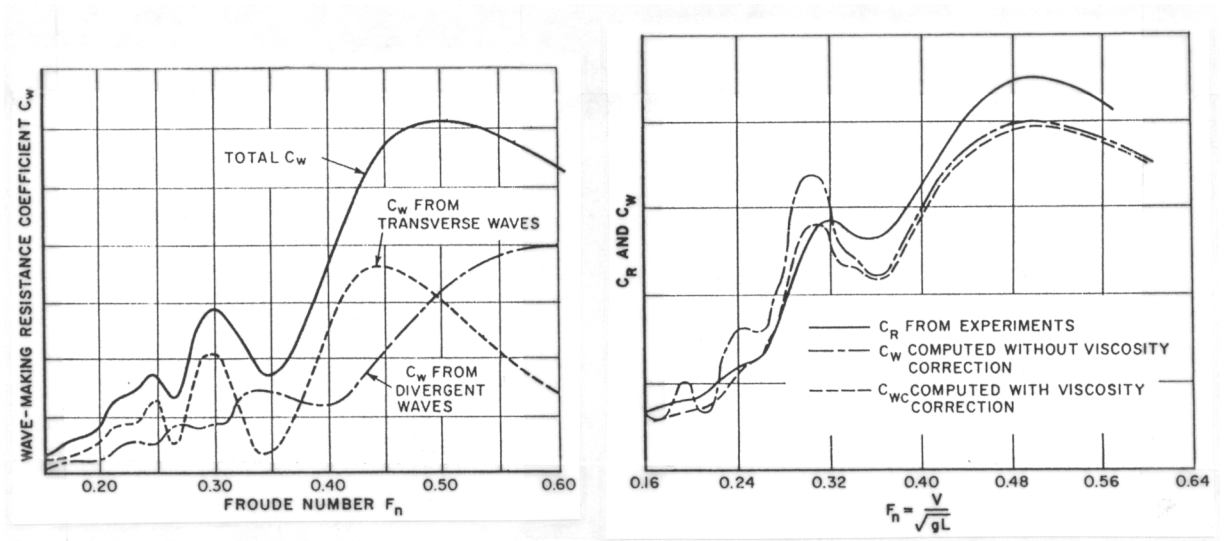


Figure 9: Typical wave making resistance coefficient plots.

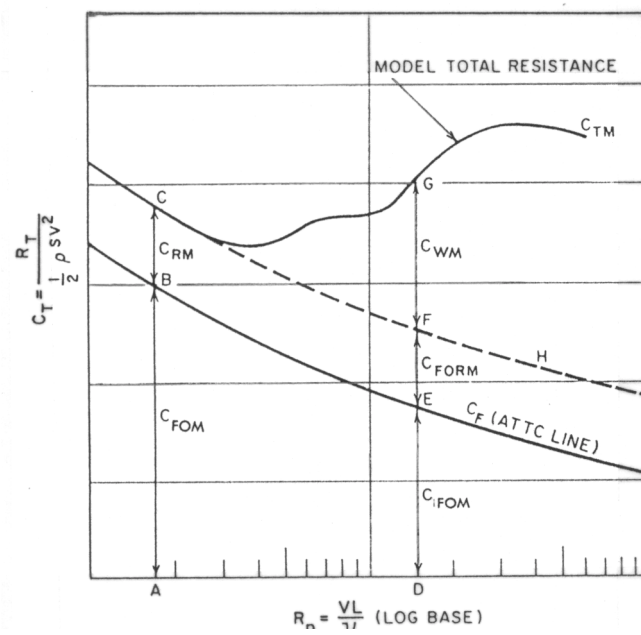


Figure 10: Elements of model resistance.

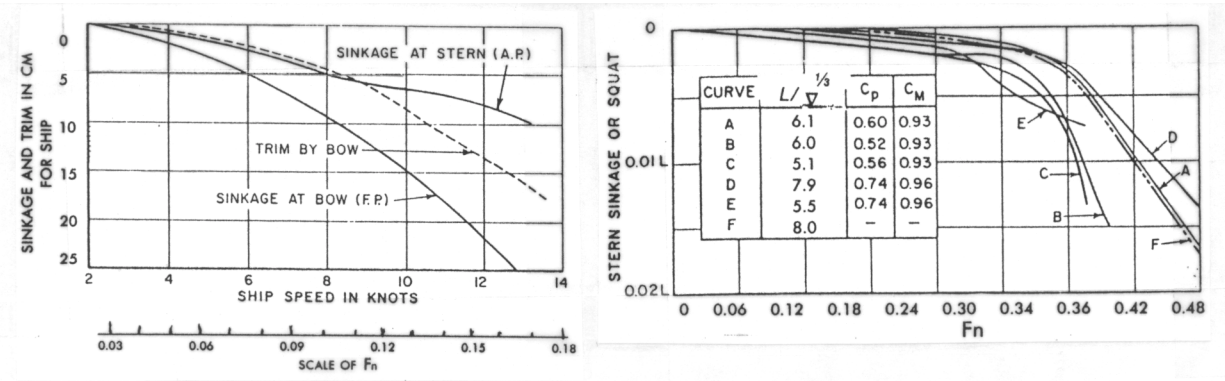


Figure 11: Changes in sinkage and trim with speed.

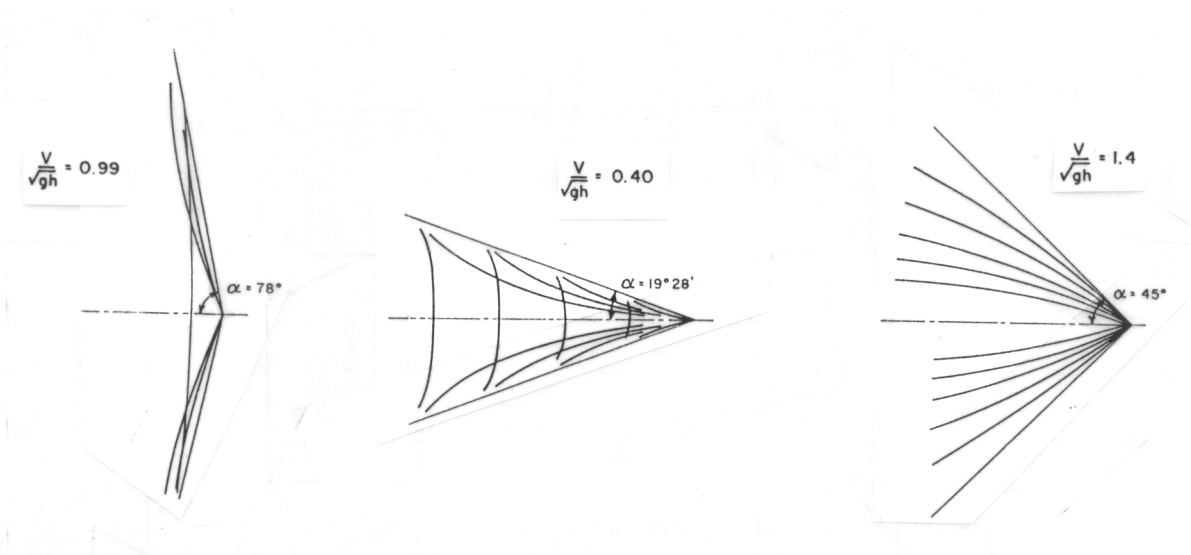


Figure 12: Effect of shallow water on wave pattern.

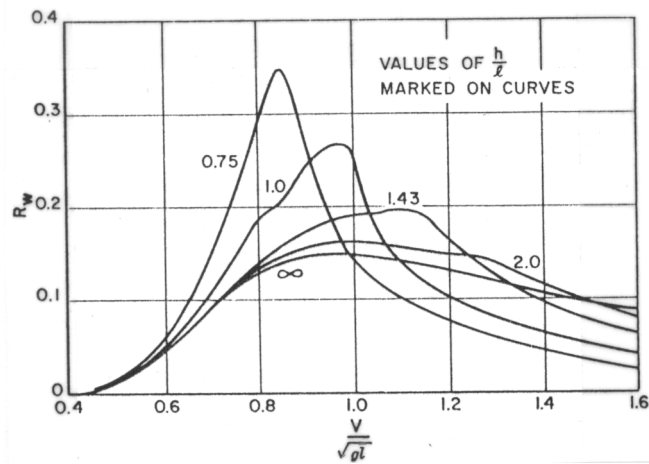


Figure 13: Effect of shallow water on wave resistance.

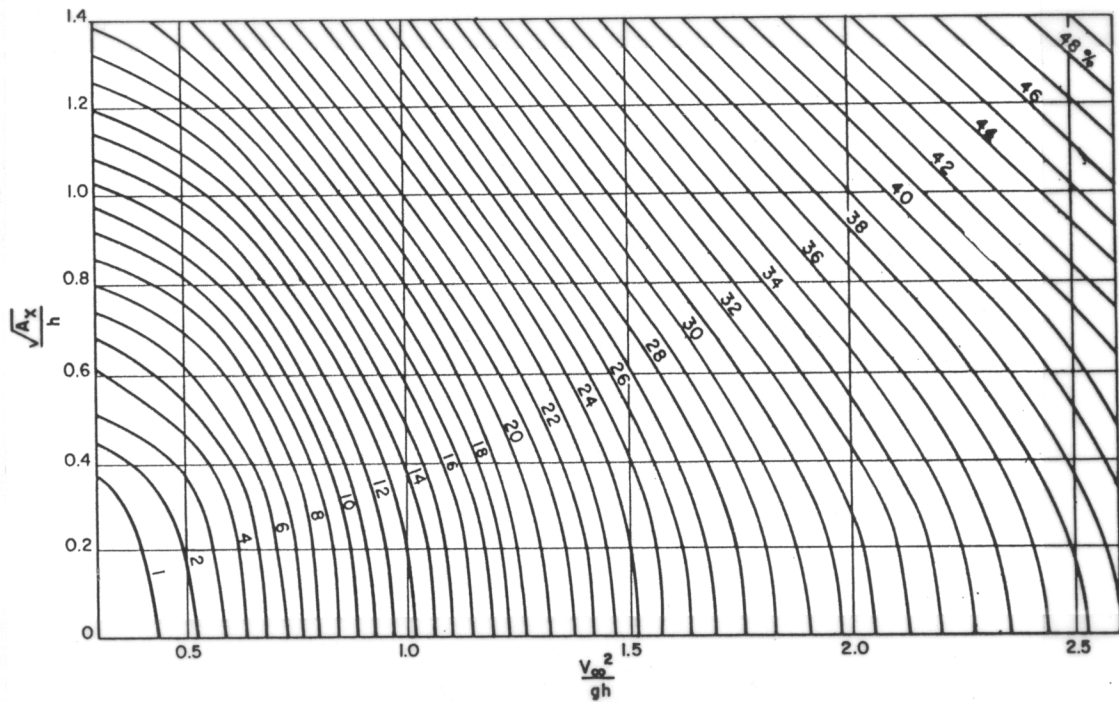


Figure 14: Chart for calculating reduction in speed in shallow water.

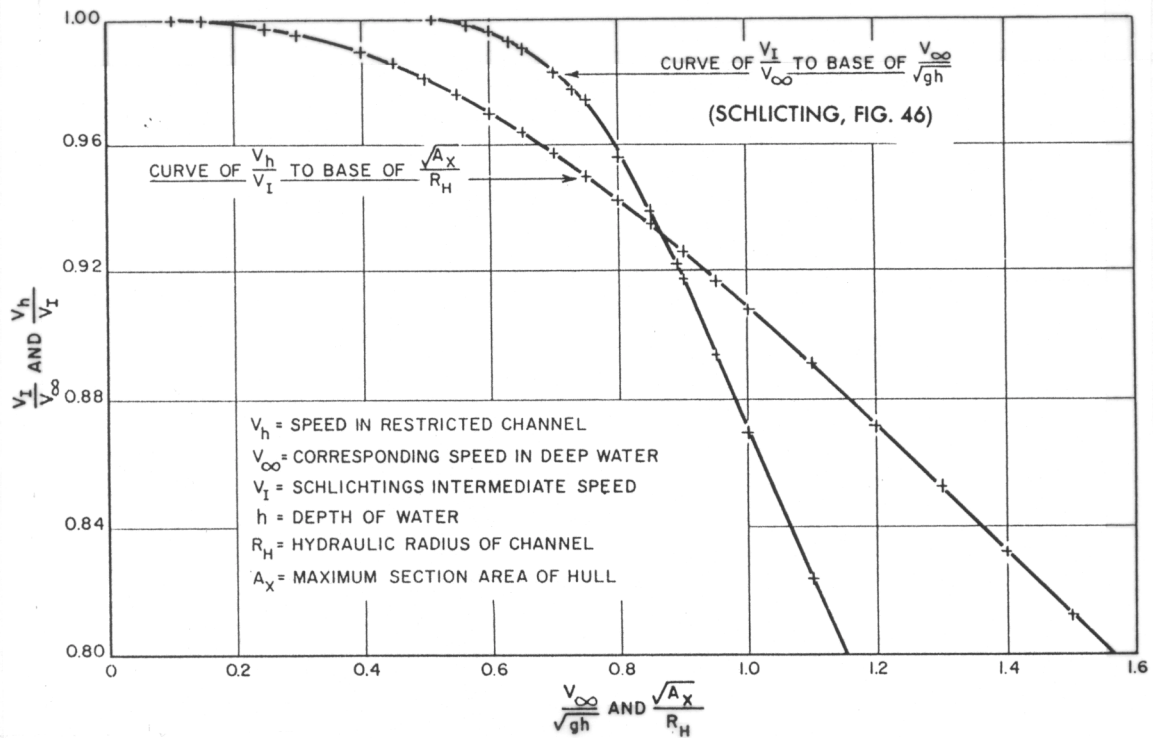


Figure 15: Curves for calculating resistance in restricted channels.

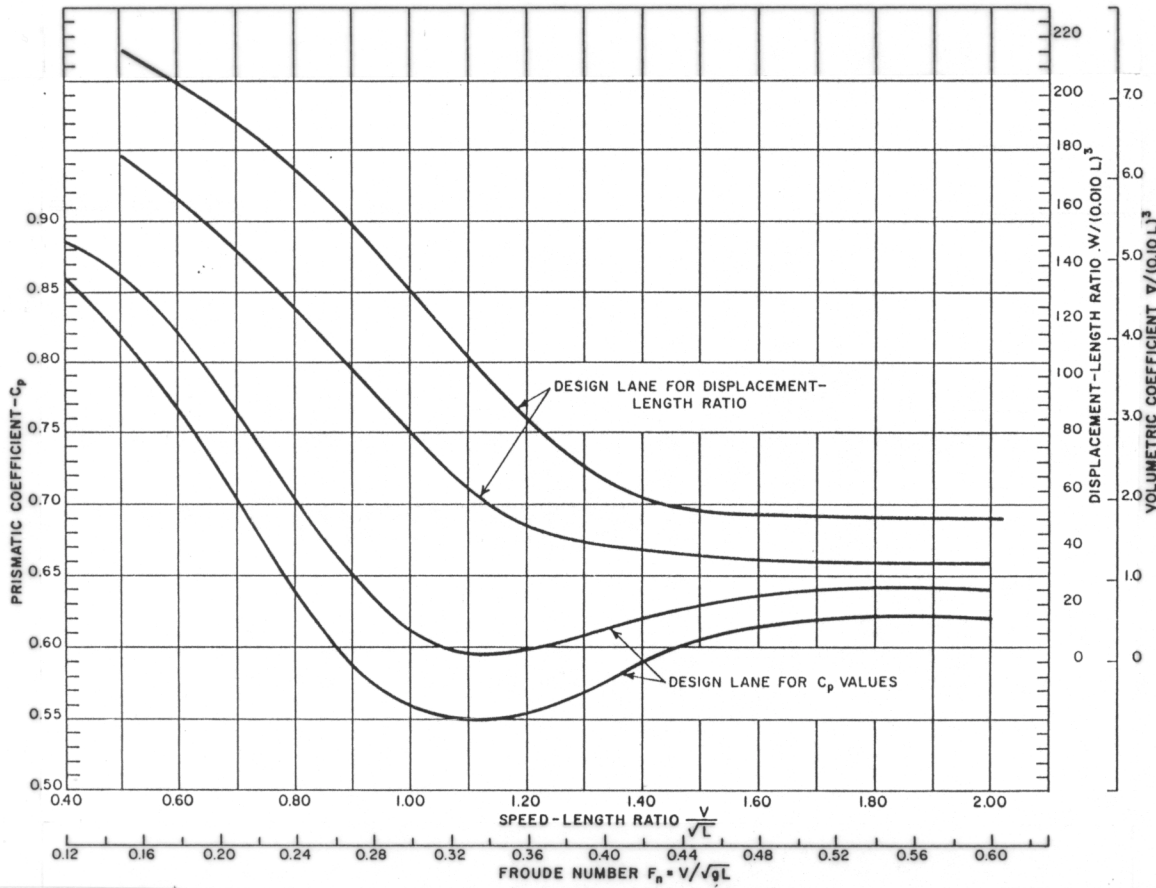


Figure 16: Design lanes for prismatic coefficient and displacement length ratio.

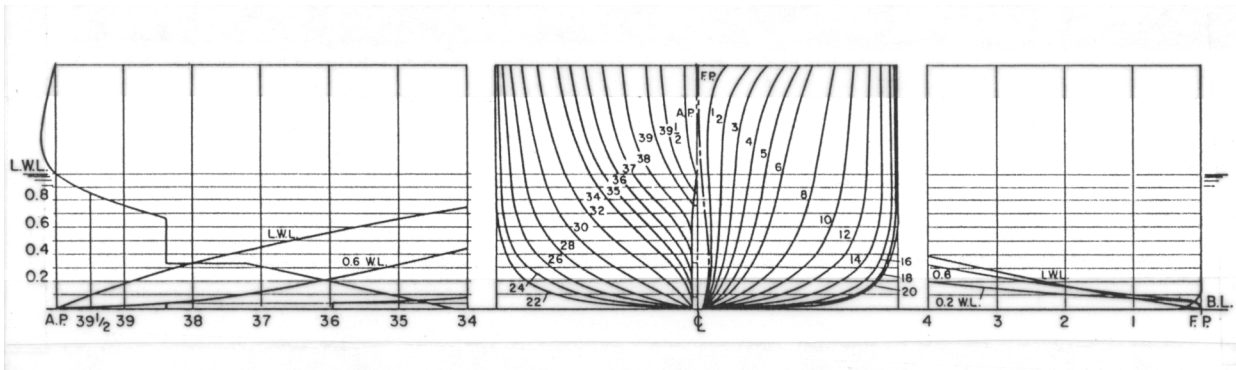


Figure 17: Lines for the parent form of Taylor standard series.

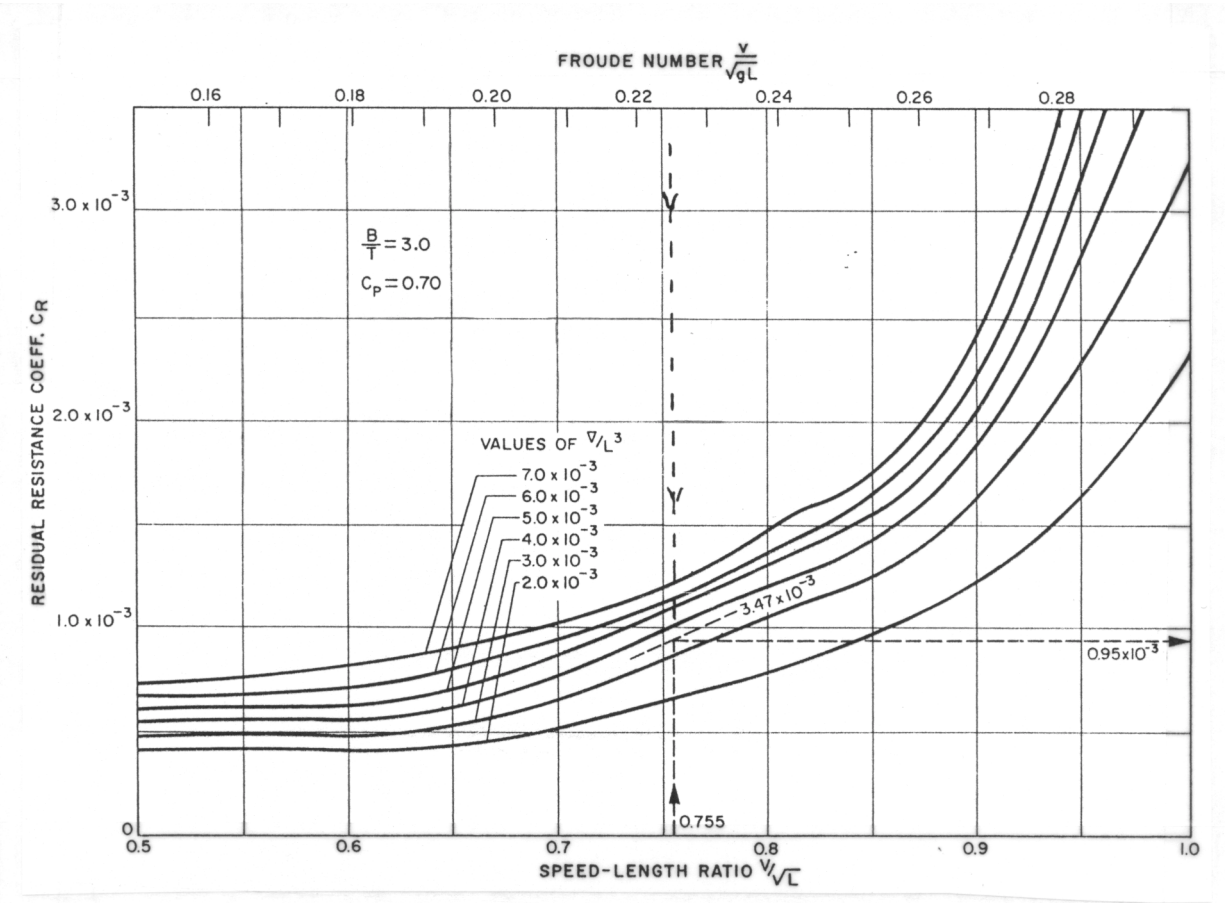


Figure 18: Typical Taylor standard series contours.

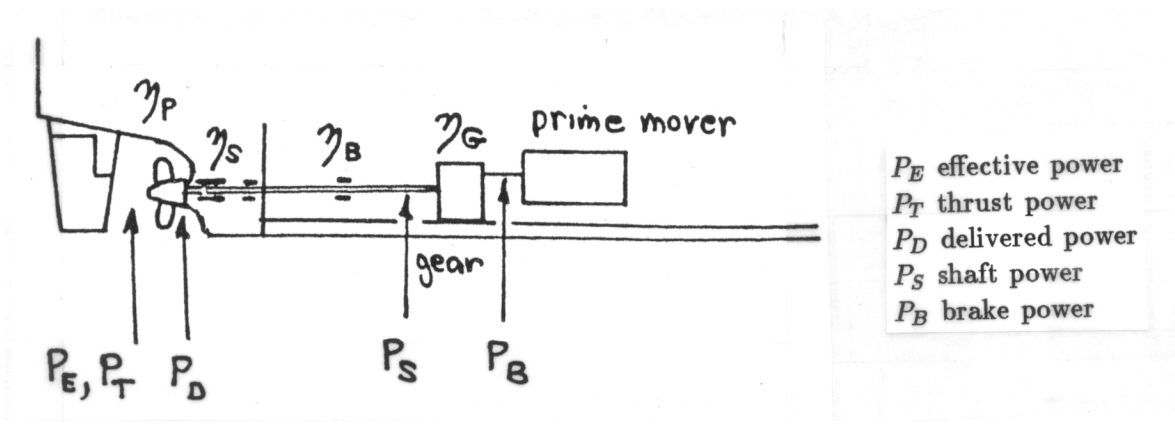


Figure 19: Ship power definitions.

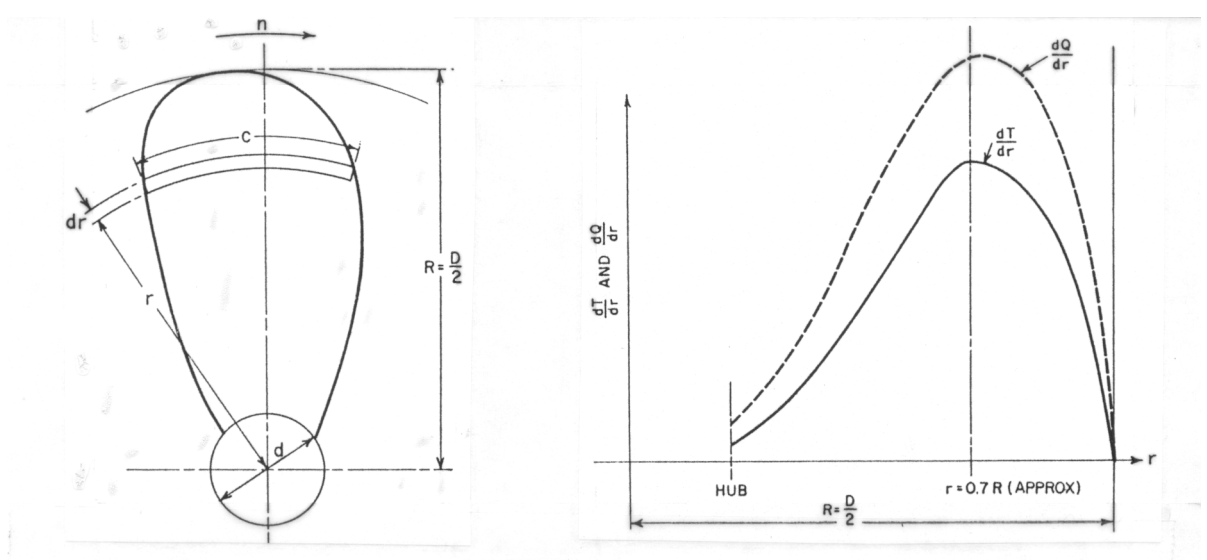


Figure 20: Propeller blade definitions and loading curves.

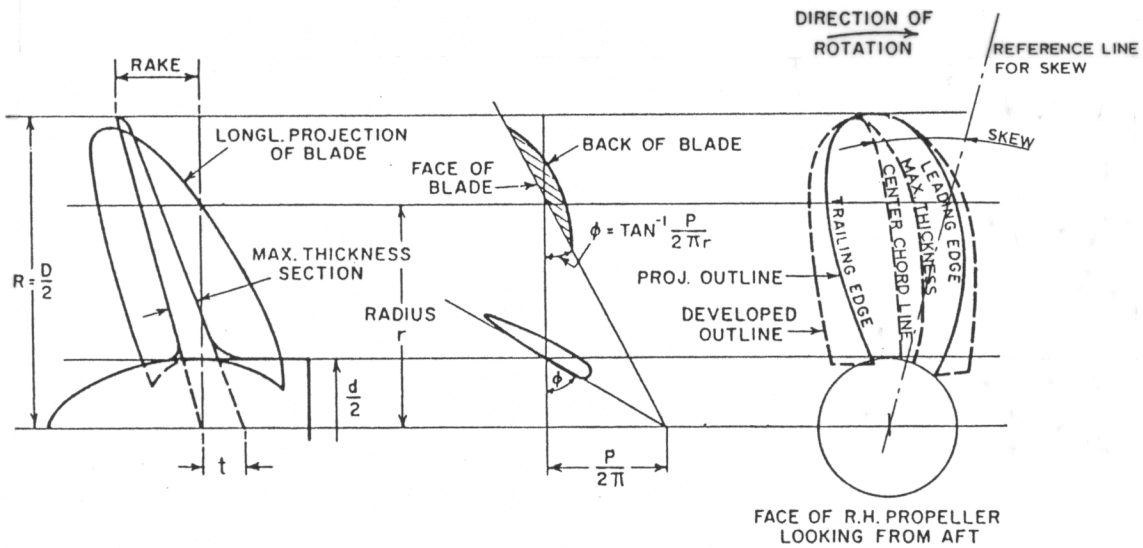


Fig. 8 Typical propeller drawing

- Diameter D Pitch ratio = $\frac{P}{D}$
- Pitch P Blade thickness ratio = $\frac{t}{D}$
- No. of blades 4 Pitch angle = ϕ
- Disk area = area of tip circle = $\frac{\pi}{4} D^2 = A_o$
- Developed area of blades, outside hub = A_D
- Developed area ratio = $DAR = \frac{A_D}{A_o}$
- Projected area of blades (on transverse plane) outside hub = A_P
- Projected area ratio = $PAR = \frac{A_P}{A_o}$
- Blade width ratio = $BWR = \frac{\text{Max. blade width}}{D}$
- Mean width ratio = $MWR = \frac{A_D / \text{length of blades (outside hub)}}{D}$

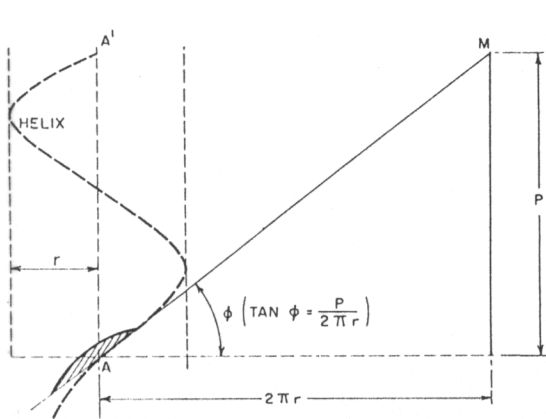
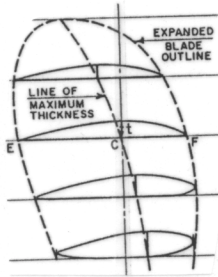


Fig. 9 Definition of pitch angle

ϕ = Pitch angle of screw propeller

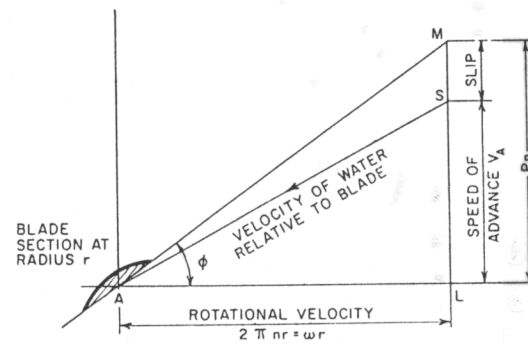


Fig. 10 Definition of slip

$$\tan \phi = \frac{Pn}{2\pi nr} = \frac{P}{2\pi r}$$

$$\text{Real slip ratio } s_R = \frac{MS}{ML} = \frac{Pn - V_A}{Pn} = 1 - \frac{V_A}{Pn}$$

Figure 21: Typical propeller drawing and definitions.

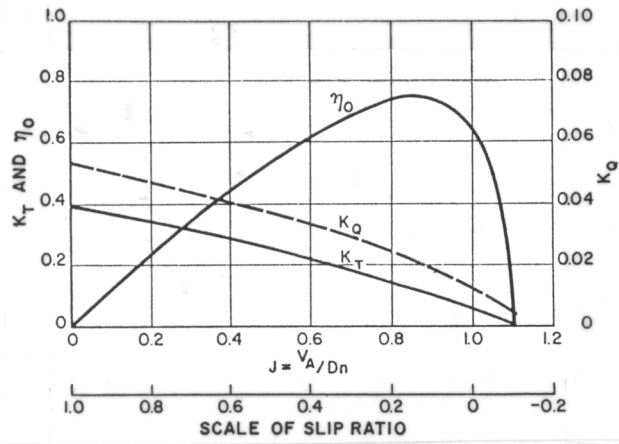


Figure 22: Typical K_T , K_Q , and η_0 curves.

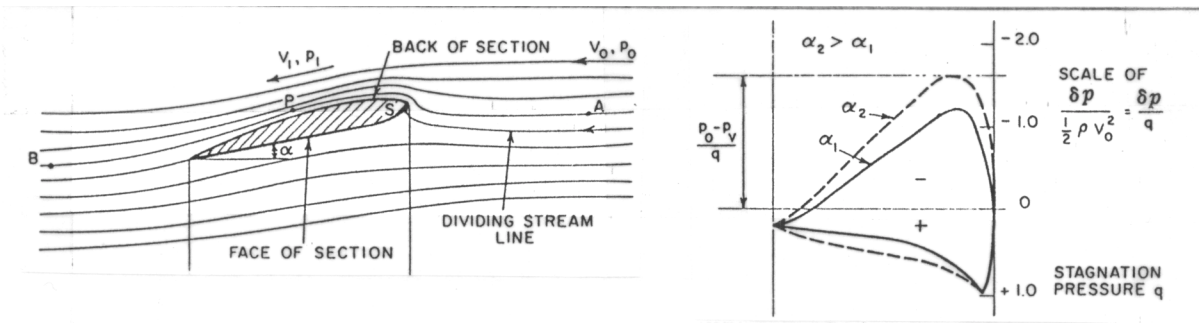


Figure 23: Flow and pressure around an airfoil.

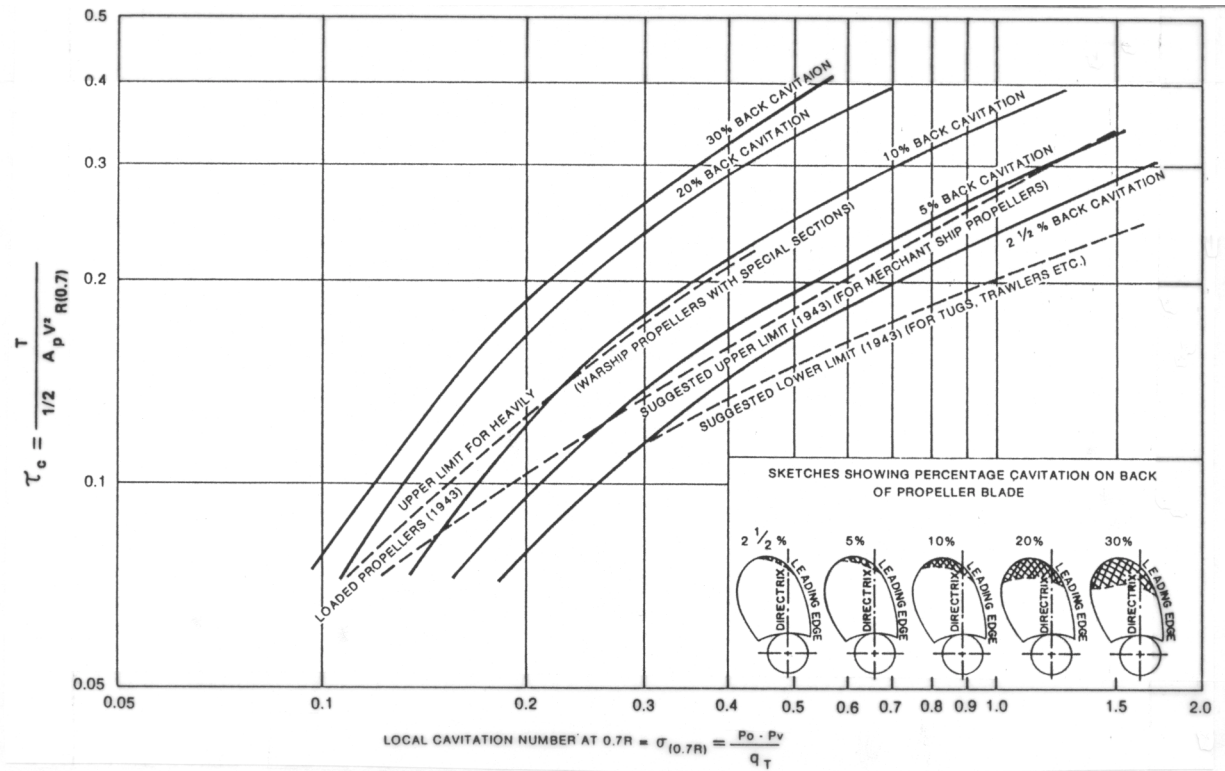


Figure 24: Burrill's cavitation diagram.

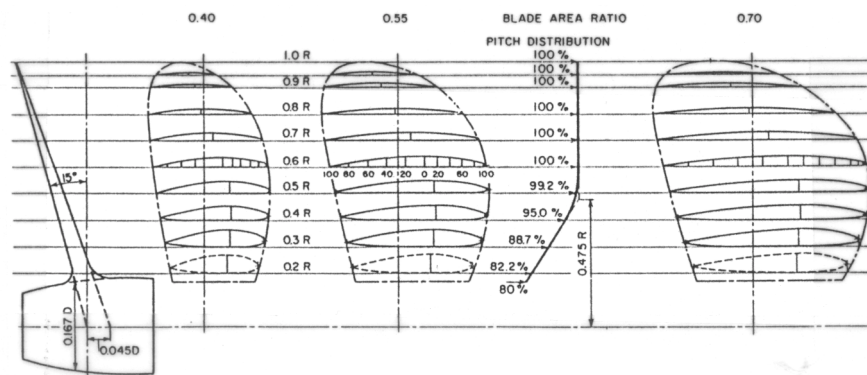


Figure 25: Blade form and sections of B.4 series.

WAGENINGEN B-SERIES PROPELLERS
 FOR 4 BLADES
 $A_E/A_0 = 0.900$
 $P/D = 0.50$ TO 1.40

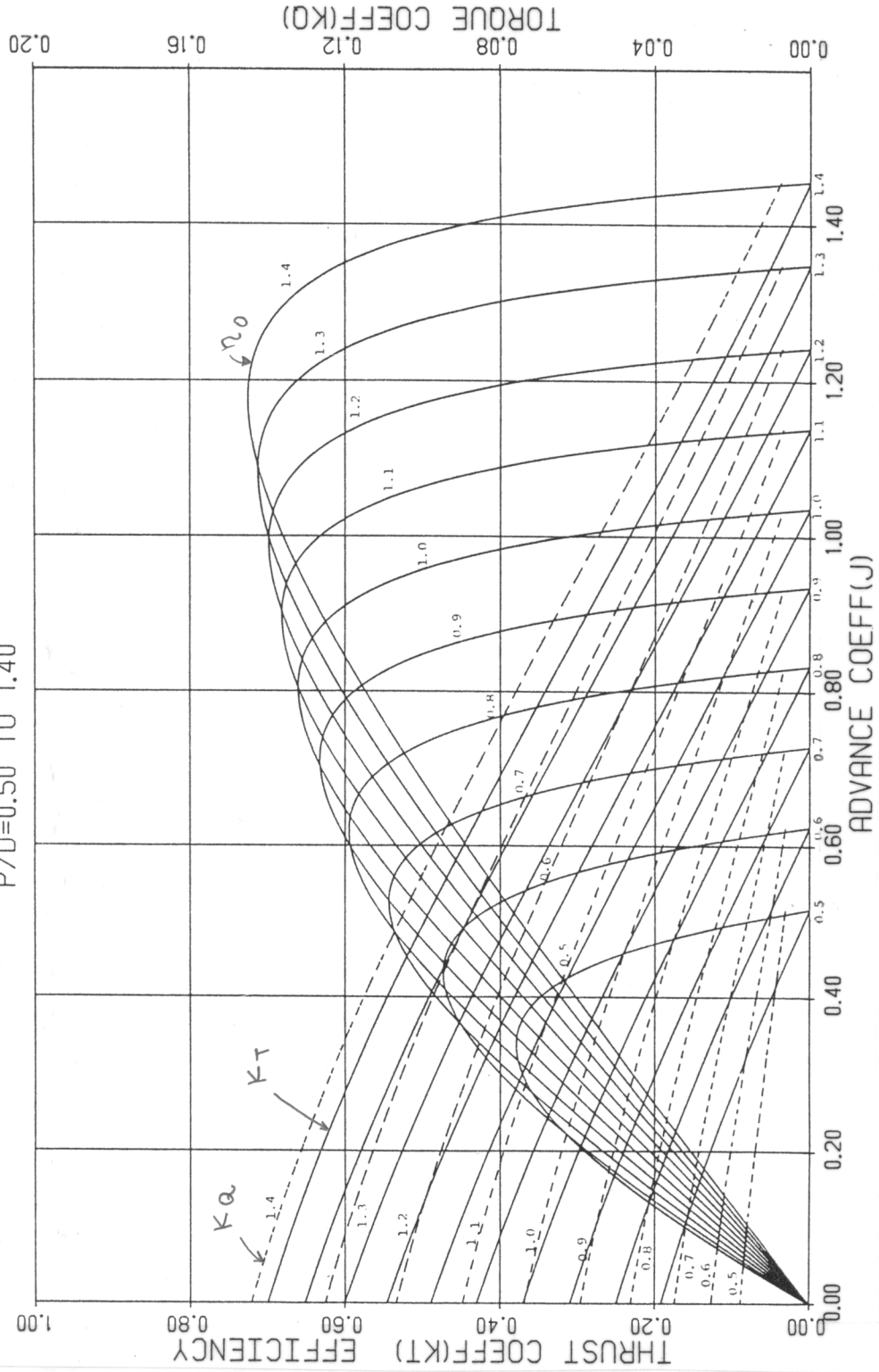


Figure 26: Wageningen B-series propeller: $Z = 4$, $A_E/A_0 = 0.9$, $P/D = 0.5$ to 1.4 .

WAGENINGEN B-SERIES PROPELLERS
 FOR 5 BLADES $AE/AD = 0.650$
 $P/D = 0.50$ TO 1.40

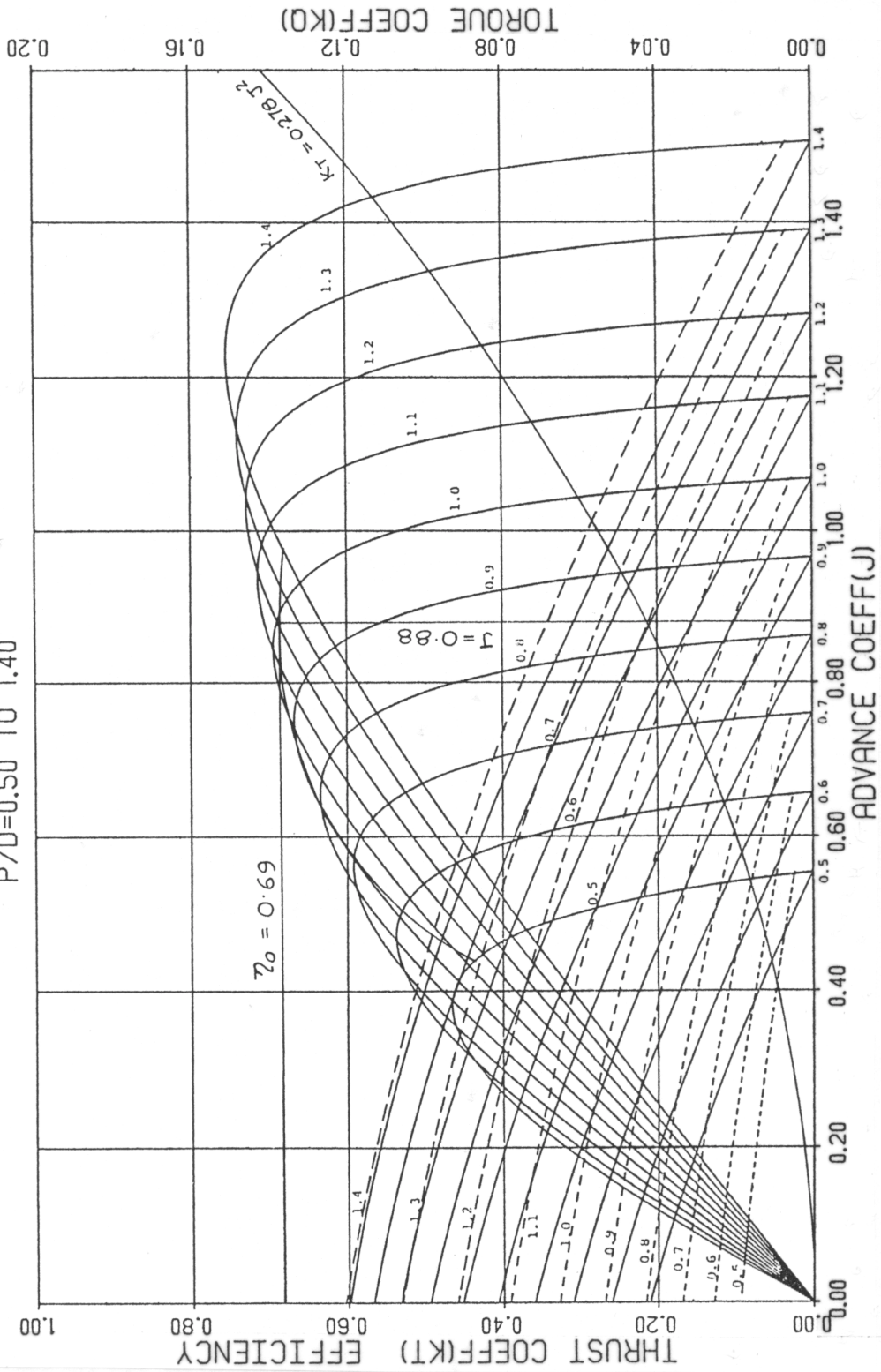
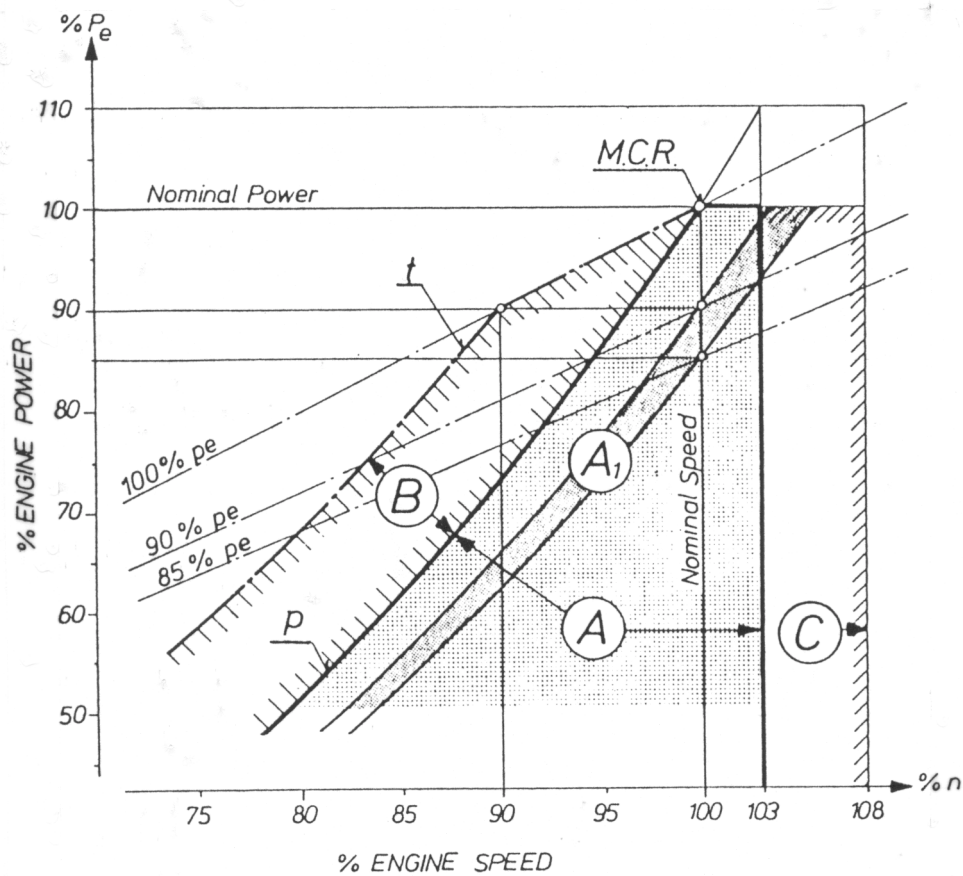


Figure 27: Example of optimal revolution propeller selection.



- A : Optimum range for continuous operation.
- A₁ : Range for engine characteristic on sea trial with fair weather, ship fully laden and clean hull.
- B : Working range for restricted time only (max. 2000 hours).
- C : Upper speed range for sea trial only.
- p : Engine characteristic on shop trial, i.e. approximated propeller curve through the point of M.C.R. Although the engine is capable of working in range B for restricted time, the aim should be to design the propeller in such a way that curve p is not exceeded in continuous service.
- t : Limitation of range B.
- M.C.R.: Maximum Continuous Rating, i.e. Nominal Power (100% P_e) at Nominal Engine Speed (100% n)
- pe : Brake Mean Effective Pressure (≅ torque)

Figure 28: Typical main engine and propeller characteristics.

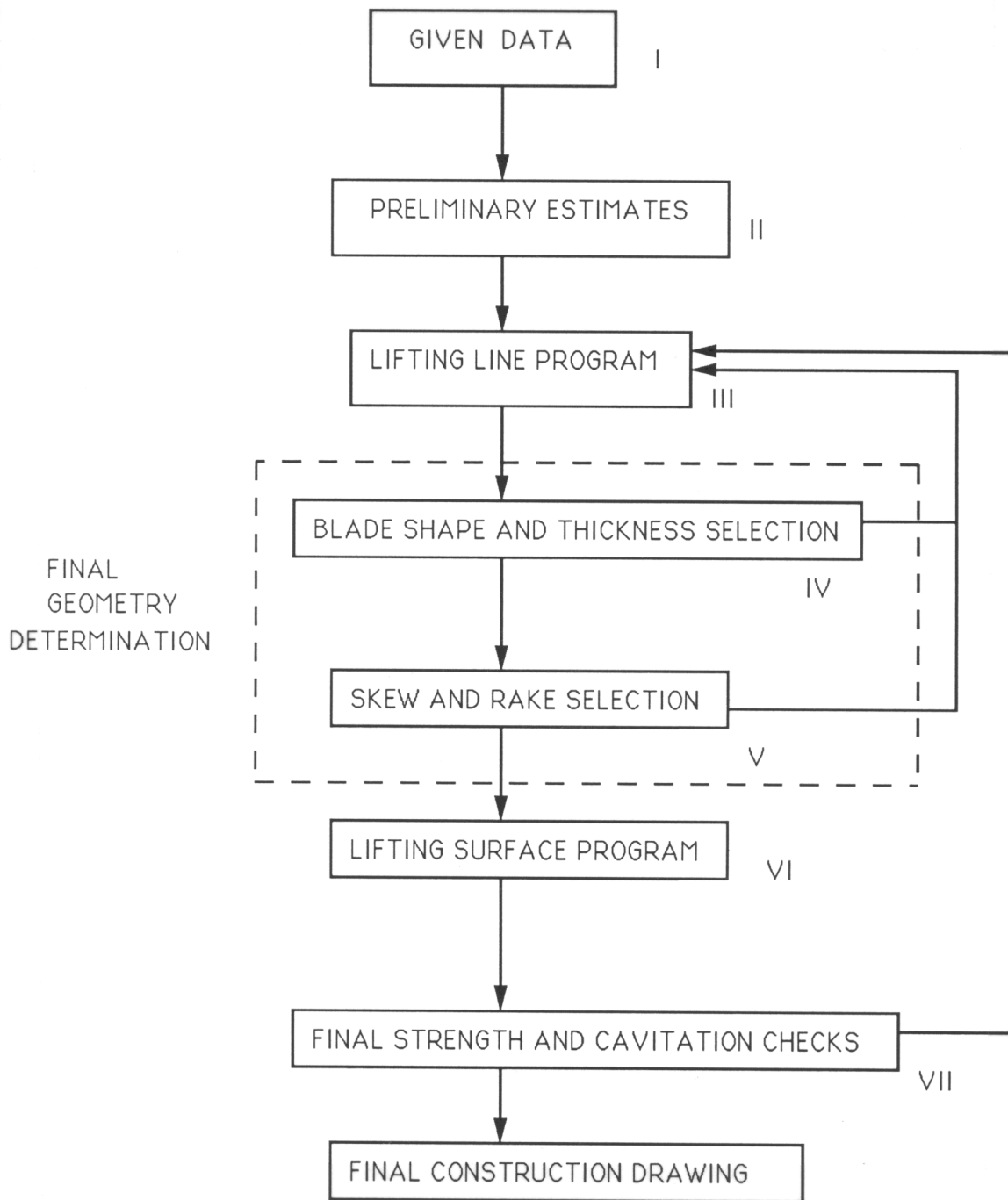


Figure 29: Theoretical propeller design steps.

Type of ship	Value of Fn		
	0.21	0.30	0.48
Large, fast, 4 screws	10-16	10-16	—
Small, fast, 2 screws	20-30	17-25	10-15
Small, medium speed, 2 screws	12-30	10-23	—
Large, medium speed, 2 screws	8-14	8-14	—
All single-screw ships	2-5	2-5	—

Table 1: Appendage resistance for various ship types.

Variables	Taylor	Series 60	BSRA
	$C_P, L/B, B/T, C_\Delta$	$C_B, L/B, B/T, C_\Delta, LCB$	$C_B, B/T, C_\Delta, LCB, L_p$
V/\sqrt{L}	0.5 to 2.0	0.4 to 1.0	0.4 to 0.85
C_B	0.4396 to 0.8018	0.60 to 0.80	0.65 to 0.85
L/B	3.92 to 17.25	5.5 to 8.5	6.89 and 7.27
B/T	2.25 to 3.75	2.5 to 3.5	2.12 to 3.95
C_Δ	26.5 to 221.6	68 to 302	114 to 385
LCF	0	-2.5 to 3.5	-0.5 to 4.05
L_p	0	0	0 to 50
propulsion	none	η_D, w, t, η_R	w, t, η_R

Table 2: Range of applicability of resistance standard series.

Blade number Z	Blade area ratio A_E/A_O													
2	0.30													
3		0.35												
4			0.40											
5				0.45										
6					0.50									
7						0.55								
							0.60							
								0.65						
									0.70					
										0.75				
											0.80			
												0.85		
													1.00	
														1.05

Table 3: Range of applicability of B-series propellers.